AD-A080 044 MPB TECHNOLOGIES INC SAINTE-ANNE-DE-BELLEVUE (QUEBEC) F/G 9/1
STUDY OF NOISE IN CROSSED-FIELD DEVICES.(U)
NOV 79 I P SHKAROFSKY, I P SINCLAIR F49620-77-C-0106
UNCLASSIFIED MPB-112-2 AFOSR-TR-80-0032 NL

| OF |
ADA
080044

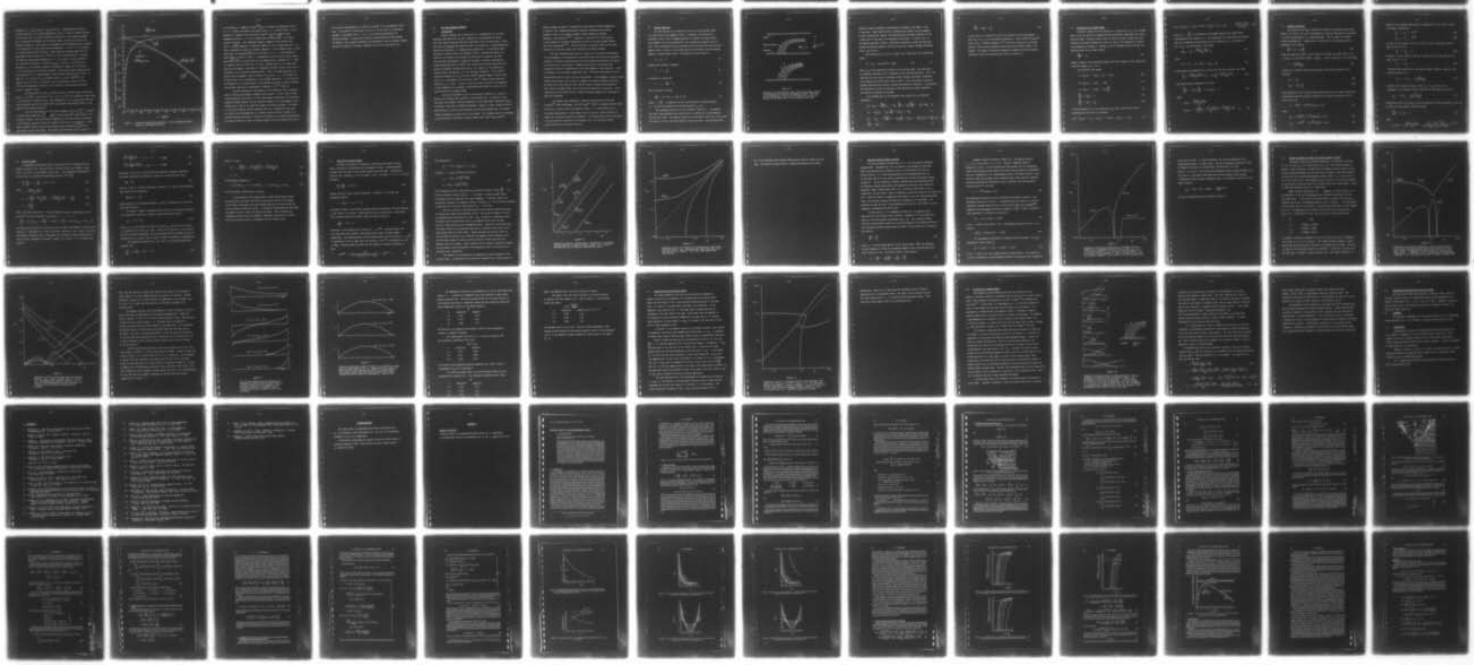

END
DATE
FILMED
2-80
DDC

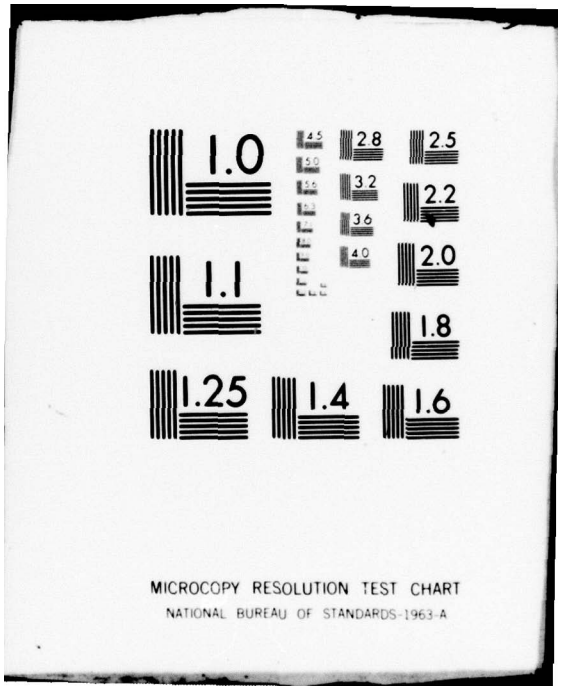
1.0
1.1
1.25
1.4
1.6
1.8
2.0
2.2
2.5
2.8
3.2
3.6
4.0
4.5
5.0
MICROCOPY RESOLUTION TEST CHART
NATIONAL BUREAU OF STANDARDS-1963-A

LEVEL II

12

MPB

MPB TECHNOLOGIES INC.

21051 North Service Road, Trans Canada Highway
P.O. Box 160
Ste-Anne-de-Bellevue, Québec, Canada H9X 3L5

MPB TECHNOLOGIES INC.
P.O. Box 160
21051 North Service Road | Trans-Canada Highway
Ste-Anne-de-Bellevue, Québec H9X 3L5 | Téléphone (514) 457-2035

12

MPB

STUDY OF NOISE IN CROSSED-FIELD DEVICES

I.P. Shkarofsky
Ian P.W. Sinclair

Final Technical Report
November, 1979

Prepared for

Director of Electronic and Solid State Sciences
Air Force Office of Scientific Research
United States Air Force
Bolling Air Force Base
D.C. 20332, U.S.A.

Under

U.S. Contract No. F49620-77-C-0106
C.C.C. Contract No. 13SR70C9-76-1
C.C.C. Serial No. 7SR77-00013

MPB Report No. 112-2

Approved by:

M.P. Bachynski
President
MPB Technologies Inc.

UNCLASSIFIED

(19) REPORT DOCUMENTATION PAGE

READ INSTRUCTIONS BEFORE COMPLETING FORM

(18) 1. REPORT NUMBER: AFOSR-TR-80-0032

2. GOVT ACCESSION NO.

3. RECIPIENT'S CATALOG NUMBER

4. TITLE (and Subtitle): Study of Noise in Crossed-Field Devices (6)

5. TYPE OF REPORT & PERIOD COVERED: (9) Final Technical Report (15) Apr 77 – 30 Sep 79

6. PERFORMING ORG. REPORT NUMBER: (14) MPB-112-2

7. AUTHOR(s): (10) Issie P. Shkarofsky, Ian P.W. Sinclair

8. CONTRACT OR GRANT NUMBER(s): F49620-77-C-0106 (15) ONR No. 13SR.70C9-76-1

9. PERFORMING ORGANIZATION NAME AND ADDRESS: MPB Technologies Inc., Ste. Anne de Bellevue, Quebec, H9X 3L5

10. PROGRAM ELEMENT, PROJECT, TASK AREA & WORK UNIT NUMBERS: (16) 2305/C1 (17) 61102F (12) 82

11. CONTROLLING OFFICE NAME AND ADDRESS: Air Force Office of Scientific Research, Directorate of Electronic and Solid State Sciences, NE Bldg.410 Bolling Air Force Base, Washington, D.C. 20332

12. REPORT DATE: (11) 30 Nov 79

13. NUMBER OF PAGES: 94

14. MONITORING AGENCY NAME & ADDRESS(if different from Controlling Office)

15. SECURITY CLASS. (of this report): Unclassified

15a. DECLASSIFICATION/DOWNGRADING SCHEDULE

16. DISTRIBUTION STATEMENT (of this Report)

Approved for public release, distribution unlimited.

17. DISTRIBUTION STATEMENT (of the abstract entered in Block 20, if different from Report)

18. SUPPLEMENTARY NOTES

19. KEY WORDS (Continue on reverse side if necessary and identify by block number)

microwave devices
crossed-field devices
interaction region
numerical analysis
dispersion relations
velocity noise
kinetic analysis in crossed fields
space charge effects

20. ABSTRACT (Continue on reverse side if necessary and identify by block number)

This research effort addresses the fundamentals of noise in electron beams in crossed field microwave tubes. Recent evolvement of new applications for DOD requires tubes with better noise characteristics in addition to the higher bandwidth and gain characteristics of crossed field devices. Much work was expended in this type of research up to 1969 but thereafter concepts have remained neglected and unexplored until 1977 when efforts were renewed. The approach here is to re-examine the analyses using simple models, to

DD FORM 1 JAN 73 1473 EDITION OF 1 NOV 65 IS OBSOLETE

UNCLASSIFIED

SECURITY CLASSIFICATION OF THIS PAGE (When Data Entered)

393 084

resolve various unknowns and gaps in knowledge and to investigate original unexplored avenues with which we can gain more insight into the mechanisms of fluctuation and modulation in electron beams travelling in crossed electric and magnetic fields.

In the first year's effort, expressions were derived based on kinetic theory for the seven moments over the energy distribution function in a plasma thermionic diode with crossed electric and magnetic fields, both for the space-charge limited and magnetic-field limited situations. The expressions are given as integrals over the distribution function at the cathode surface, whose form is left arbitrary. Analytic results, valid in the region of the potential minimum, are provided in the space-charge limit when the potential profile is assumed to be parabolic in the vicinity of its minimum. The seven moments are the density profile, the two current flux components, the two mean velocity components and the two mean square velocity components. From the latter four moments, the velocity noise is determined. At the potential minimum, the velocity noise is minimized when $\omega_{pm}^2/\omega_c^2 = 2$ where ω_{pm} is the plasma frequency at the potential minimum and ω_c is the cyclotron frequency, and operation under this condition is recommended. It is also shown how Lindsay's, Ho and Van Duzer's and the present analyses are related to each other.

In the current year's effort, we concentrated on applying the moment macroscopic equations to investigate the propagation of fluctuations in crossed fields. For the electron gun region, the differential equations were derived for accelerated beams being bent by the magnetic field. As a start in computational analysis, we concentrated our attention on the interaction regions. Here the nature of straight electron beams with finite width and transverse velocity gradient was explored using the model of Buneman et al. Curves were generated of dispersion relations using a numerical eigenvalue scheme and compared with Buneman's analytical results.

TABLE OF CONTENTS

1.0 RESEARCH OBJECTIVES

1.1 Tasks and Work Statement

The contractor shall furnish scientific effort needed to conduct research directed towards the following areas:

(a) An electronic equation involving differential equations will be derived for the modulation quantities in a linear crossed-field M-type device, which will include the dc variations in the beam parameters.

(b) The above relation will be applied to investigate the growth of noise in the transition from the gun region to the slow-wave structure region, including dc space-charge effects near the cathode.

(c) The relation will also be applied in the drift region between parallel plates and the related diocotron instability will be investigated.

(d) Parameters in the theory will be varied with the aim of reducing the noise content. Possibilities include smooth and abrupt velocity variations and various cathode lengths and geometries.

(e) Kinetic theory, using the electron velocity distribution function and the Vlasov equation , which includes the thermal spread of the beam, will be investigated for the dc beam parameters and then for the above four tasks on the modulation quantities in the beam.

(f) A hybrid approach to investigate noise will be carried out in which the kinetic theory approach will be applied in the region between the cathode and potential minimum leading to noise boundary

conditions at the potential minimum while the electronic equation will be applied in the succeeding region.

(g) If the indications justify the following, theoretical investigations will be performed on new cathode and gun structures, attempting to eliminate the above mentioned problems. These techniques include velocity jump transformers, shortening the cathode length, tilting the cathode with respect to the magnetic field, cold cathode operation and artificial means of controlling or eliminating the potential minimum in front of the cathode.

1.2 Work Completed

During the first year we have investigated parts of tasks d, e, and f, mainly part f. In the second year, our effort was directed towards tasks a, b, c, particularly c. In the future work, we propose to concentrate on tasks b, d, f, and g. The macrospic moment approach will be pursued intensively, since it is simpler to apply for analytical results. Generally, the objective is to investigate the growth of noise in crossed fields as the beam propagates through various structures, such as the gun region, drift region or circuit region.

2.0 INTRODUCTION

In recent years microwave tubes, especially klystrons and magnetrons, have been made more efficient and lighter[1] giving solid state sources strong competition. Magnetrons have been very flexible in adapting tube designs to systems requirements[2]. For example, Varian Associates now has a 1 MW S-band tube which can be replaced in a fixed cavity structure. High gain, to 30 dB, has been achieved in CFA (crossed-field amplifier) devices by Northrop Corporation, while bandwidth is over half an octave at 3 Kw. Increased gain means that overall system costs and complexity can be reduced by using fewer driver stages. Tube lifetime has also been extended, being as high as 8-10,000 hours for distributed emission tubes[3]. In future years, reliability of tube systems will be increased[4] and the frequency range will be extended into the mm range as gyrotron tubes are developed[5]. This latter tube is projected to yield power output in the multikilowatt range[1], and may be applicable to solar-power satellite-to-ground power transmission[6] as well as energy injection into tokamaks for fusion[1].

While engineers extend lifetime, power and frequency range of microwave tools, fundamental research into the nature of the cathode surfaces, potential distributions and electron beams has been continuing apace. While magnetron-type electron guns are used in CFA devices, they are also applicable to the generation of the hollow, cylindrical beams used in gyrotrons[1]. These beams are expected to allow 40% conversion efficiency because of optimized interaction with the RF field. Electron gun design and beam voltage are therefore critical parameters. Beam trajectories have been modelled on computers, both for gyrotrons[7] (IEEE Trans-ED. issue June 1977) and for CFA devices[8]. With such codes it is possible to alter beam-shaping electrodes and study the effect on electron beam shape.

Trajectory analysis necessarily involves a close knowledge of the potential distribution within the gun region of the given device. Kino (1960)[9] designed a "short gun" with a cathode short relative to the cycloid length, and a "long gun"

for increased power. Masnari and Rowe (1965)[10] used a technique developed by Lomax[11] and Kirstein[12] to calculate the electrode shapes and potentials required to produce a laminar, or Brillouin, electron beam in the short Kino gun. More recently, True (1978)[13] presented numerical analyses of potentials within Kino guns, using a deformable mesh. Such analyses, although in two dimensions, are realistic approximations to the actual conditions within an electron gun.

Fontana, MacGregor and Rowe (1979)[14] have developed an improved two-dimensional computer simulation of a Kino gun, using 5-10,000 representative electrons. The potential distribution is that of True [13], and includes secondary emission from the cathode. Two methods are used to advance the trajectories: in the static calculation, convergent solutions are found between successive solutions of Poisson's equation, while in the time-dependent calculation no such steady state is sought. They analyze several types of electron guns, including the short and long Kino guns. Convergent solutions were found readily for the short Kino gun but for the long gun returning cycloiding electrons rendered convergence unattainable. For this latter case, the time-dependent model proved successful.

Since 1964 much empirical work has been done on reducing the noise level in the long Kino gun. In view of their light weight, high power and wide bandwidth, reducing the noise level in injected beam devices is expected to go a long way toward improving their scope of use. To this end, Fontana et al have been developing their two-dimensional model, while Kooyers and Shaw (1979)[15] have produced a three-dimensional model using a slightly simplified geometry. They have developed a Lagrangian particle simulation code capable of modelling up to 20,000 electron charges. The electrons are emitted from the cathode with random velocity, number and position, and from their subsequent positions

and velocities, current and velocity fluctuations (noise) are calculated. They define a "space charge smoothing factor" Γ, as ratio of root mean square fluctuation at gun exit to rms fluctuation at the cathode; Γ is found to be ~ 1.75 in the temperature limited case, and ~ 0.2 in the space-charge limited case.

The ultimate source of the noise in a CFA is the randomness in the emission current density leaving the cathode surface[16]. Trajectory modelling is one way of mapping the development of noise from cathode to gun exit. However, the mechanisms of fluctuations in electron beams can be solved best by a consideration of the motion of particles in cross-fields near the potential minimum using kinetic theory. On the other hand, the propagation of noise can be most readily investigated by a consideration of the field equations associated with the beam together with the equations of motion.

In the first year's work, we successfully analyzed using kinetic theory the velocity noise in crossed fields near the potential minimum. We derived a basic condition on density and magnetic field to minimize the mean square deviation in velocity. This work is reported in Section 3.

In the recent year's work, we undertook to investigate the full equation approach, reported here in Section 4.

3.0 VELOCITY NOISE IN CROSSED FIELDS

3.1 Summary

A detailed description of this phase of the work is provided in the published reprint reproduced in Appendix I. Here we briefly summarize the results.

We investigate both the space-charge limited case and the magnetic field limited case in a thermionic diode with crossed electric field along the x-direction and magnetic field along the z-direction. By a careful systematic analysis based on an assumed parabolic spatial variation in the potential about the space-charge minimum, we clarify several aspects on the operation of a space-charge limited diode with a transverse magnetic field and we obtain simple but important results for the noise in the velocity components.

In the first part of the analysis, we illuminate Lindsay's[17,18] (1960, 1964) considerations on the velocity regions over which we have to integrate the velocity distribution function to derive the moments or integrals over this distribution. Let subscript zero refer to the initial velocities w_{xo} and w_{yo} at the cathode upon emission. Without subscript zero, the velocities (w_x and w_y) refer to those at position X within the diode. The equivalence between the (w_{xo}, w_{yo}) and (w_x, w_y) planes as far as the regions and limits of integration are identified and mapped both in the space-charge and magnetic field limited situations.

For the space-charge limited case, Lindsay[18](1964) however did not make much headway since his integrals could not be manipulated before the space potential distribution was known. Working in the (w_{xo}, w_{yo}) plane, we illustrate a number of new features, upon assuming the potential to have a parabolic spatial variation about the potential minimum. (We also justify this assumption by generalizing somewhat the results).

In relation to the emission current flux, J_x, perpendicular to the electrodes, we prove that

a) our formual reduces to Lindsay's[18](1964) if one inserts our assumed parabolic potential variation into Lindsay's equation,

b) the result in Ho and Van Duzer[19](1968), also for a parabolic spatial variation in potential, agrees with our result if we allow the anode to receed to infinity, as they do,

c) and thereby we have clarified the relationship between Lindsay's and Van Duzer's analyses.

General relations are derived for seven moments in terms of integrals over the two-dimensional electron velocity distribution function, both for the space-charge limited and magnetic field limited situations. The distribution function refers to its value at the cathode but its form is left arbitrary, except for the assumption that it is a function of the magnitude of $w_{xo}^2 + w_{yo}^2 + w_{zo}^2$. The seven moments are the current fluxes, J_x and J_y, the electron density, the mean velocities, $\overline{v_x}$ and $\overline{v_y}$, and the mean square velocities, $\overline{v_x^2}$ and $\overline{v_y^2}$. For the space-charge limited situation, we effect major simplifications upon adopting all of Ho and Van Duzer's [19](1968) assumptions. That is, besides using a parabolic potential, the reasonable assumptions are also made that the potential minimum is very close to the cathode and very far away from the anode. With these assumptions, the relations for the moments can be expressed in terms of simple integrals over the three-dimensional distribution function, which can be readily integrated for a Maxwellian form.

The cutoff characteristics of J_x versus magnetic field, B, differs markedly between the magnetic field limited case and the space-charge limited case. In the former case, J_x depends on magnetic field and anode conditions (position, potential) and it decreases abruptly above a critical magnetic field given by the

condition $(X_a - \eta_a/X_a)$ where $\eta_a = e\phi_a/kT$ and $X_a^2 = (m/2kT)(eB/m)^2 x_a^2$ where ϕ_a is anode potential, T is cathode temperature, and x_a is anode to cathode spacing. In the latter case, J_x is more affected by conditions at the potential minimum and its decrease with magnetic field is much slower. Before the action of the potential minimum on J_x was known, the broadened cutoff characteristic was thought to be indicative of a very high electron temperature. In fact, it is a property of a space-charge limited situation. These analytical concepts agree with the experimental work of Bacal et al [20](1970) on cutoff characteristics. We denote the important space-charge parameters by β. It is equal to $-\eta_m/X_m^2$ generally. For a parabolic potential, β is given by ω_{pm}^2/ω_c^2 where ω_c is the cyclotron frequency, ω_p is the plasma frequency and subscript m means that the quantity is to be evaluated at the potential minimum. Space-charge limited conditions are characterized by $\beta > 1$, whereas magnetic field limited conditions occur when $\beta < 1$. When $\beta > 1$, the current flux J_x decreases slowly as $J_s[(\beta - 1)/\beta]^{\frac{1}{2}} e^{\eta m}$ as the magnetic field $(B \propto \beta^{-\frac{1}{2}})$ is increased. Also its magnitude is down by a factor $e^{\eta m}$ from the temperature limited J_s value, similar to space-charge conditions without a magnetic field.

The new relation for the J_y current flux for the space-charge limited case, gives $J_y = J_s \beta^{-\frac{1}{2}} e^{\eta m}$. The rms sum, $(J_x^2 + J_y^2)^{\frac{1}{2}} = J_s e^{\eta m}$, has an identical form to that in the absence of a magnetic field. This dependence for J_y is again quite different from calculated results by Lindsay[21](1962) and Lindsay and Goodwell[22](1965) in the magnetic field limited situation.

From the relationships for the velocity moments, $\overline{v_{x,y}}$ and $\overline{v_{x,y}^2}$, we obtain the mean square deviations, $\overline{v_{x,y}} - (\overline{v_{x,y}})^2$, and in particular their values at the potential minimum. The noise velocity components are the mean square fluctuations of the velocity components which are created by shot noise in the emission. Using Rack's (1938)[23] theory, we relate the velocity noise components, $\overline{\langle v_{x,y}^2 \rangle}$ to the mean square velocity deviations. The results are illustrated here in Figure 3.1.

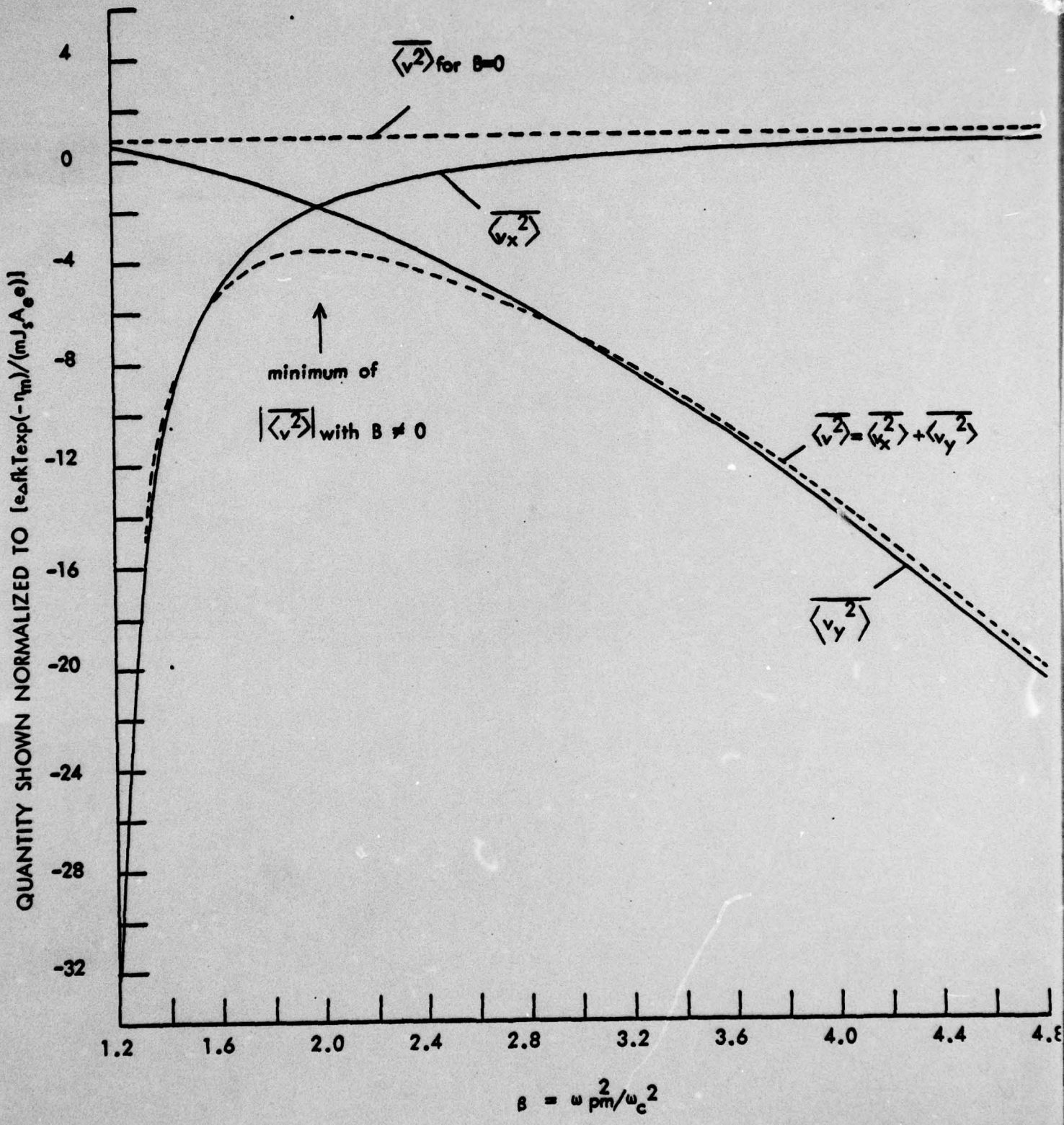

Figure 3.1: Variations of Mean Square Deviations, x and y Components and Sum, Versus β at the Potential Minimum.

In the absence of a magnetic field, $\overline{\langle v^2 \rangle}$ has the familiar multiplicative factor $(4 - \pi) = 0.8584$, (See Smullin and Haus[24], 1959, p. 17, or Rack[23], 1938). In the presence of a magnetic field, Van Duzer (1963)[25] uses the magnetic field independent factors $(4 - \pi)$ and 2 respectively for $\overline{\langle v_x^2 \rangle}$ and $\overline{\langle v_y^2 \rangle}$. Our results are much different. Both components depend on magnetic field through the β factor. The $\overline{\langle v_x^2 \rangle}$ component is large and negative for low β values near one. Its value, normalized as shown in the graph, approach $4 - \pi$ as β becomes large. On the other hand, the normalized $\overline{\langle v_y^2 \rangle}$ starts off when $\beta = 1$ at $4 - \pi$ and decreases to large negative values for large β. Considering the total velocity noise content, namely $\overline{\langle v_x^2 \rangle} + \overline{\langle v_y^2 \rangle}$, the graph shows that its magnitude has a minimum at $\beta = 2$ where its numerical factor is $2\sqrt{2}(5-2\pi) = -3.629$. Although this is 4.23 times worse than the zero-magnetic field value, it represents the least velocity noise that is obtainable at the potential minimum position. Thus for optimum operation, one should allow the magnetic field to satifsy $\beta = \omega_{pm}^2/\omega_c^2 = 2$. In all cases, the velocity noise is also proportional to the cathode temperature. If the tube can be operated with no cathode heater, this broadband noise will be greatly reduced. This probably explains the experiments of Bespalov et al[26,27] (1967a,b).

The main limitation in the analysis is the assumption that the magnetic diode is either space-charge or magnetic field limited. In most cases at high current emissions, the diode is in fact space-charge limited near the cathode and potential minimum regions, but the situation changes over to the magnetic field limited case in most of the diode far beyond the potential minimum. Our result on the electron density profile indicates that such a change-over does occur. Our initial first approximation of a constant density profile, inherent in a parabolic spatial potential, is found to be incorrect in the second approximation. The electron density is found to decrease rapidly from the cathode position and,

in the second approximation, its profile is similar to the non-magnetic field case. If we define an "effective" $\beta = \omega_p^2/\omega_c^2$, we note that it is spatially dependent, decreasing from $\beta > 1$ to $\beta < 1$ at positions much beyond the potential minimum. An analytical solution, incorporating both space-charge and magnetic field limited situations, is non-existent, but an iterative computer solution is feasible to perform, although it has not yet been done by us.

4.0 THE FIELD EQUATION APPROACH

4.1 Introduction

Several problems can be solved only by a consideration of the field equations associated with the beam, together with the equations of motion. This field equation approach has been undertaken during the second year's effort. The noise is propagated and amplified under the influence of a plasma instability known as the diocotron, or slipping-stream instability. In an electron beam drifting in crossed electric and magnetic fields, a growing wave exists as a results of the velocity slip between the bottom and top edges of the beam. This has been investigated in idealized situations by several investigators, notably MacFarlane and Hay (1950)[28], who treated the Brillouin beam (with each electron following a straight path and $\omega_s = \omega_c$, where ω_s is the gradient of velocity across the beam and ω_c is the cyclotron frequency). Gould (1957)[29] treated thin beams with $\omega_s << \omega_c$, Knauer (1966)[30] analyzed beams of finite width and $\omega_s << \omega_c$, and Buneman, Levy and Linson (1966)[31] treated finite beams with arbitrary $\omega_s : \omega_c$, ratio. To date, no one has actually analyzed the propagation of this instability in a bending, converging electron beam: all effort so far has been devoted to straight beams.

The theory developed so far on the diocotron instability is unable to account for the large noise content in the long Kino gun. In addition to shot noise near the cathode, a further mechanism of noise enhancement apparently exists in the gun. Some type of feedback mechanism is thought to exist, whereby diocotron amplification of the shot noise modulates the potential minimum near the cathode, thereby increasing the noise input to the system. This feedback theory is confirmed by the observation that shorter cathode lengths yield lower noise levels[32].

Further evidence is seen in a reduction in noise when the cathode temperature is reduced. This "temperature-limited" operation eliminates the potential minimum in front of the cathode surface, thereby making the feedback mechanism less effective[26,27]. Similarly, it has been found that placing a grid between the potential minimum and the bulk of the space charge reduces the noise considerably[33,34]. The grid prevents the electric field of the noise modulation in the space charge from reaching the potential minimum.

The above considerations point out a need for an increased understanding of the propagation of fluctuations in an electron beam with varying dc parameters. Analysis of electron trajectories and the self-consistent potentials would appear to be only part of the solution. Plasma instabilities of this nature must necessarily involve a consideration of the electromagnetic field equations. Given an estimate of the zero-order quantities, then, first-order perturbations can be derived which will be closer to actual fluctuations. Electromagnetic solutions, both linear and non-linear, may be able to encompass the computer-analyzed trajectory solutions and at the same time point the way toward increased understanding of other types of electron beams, such as the hollow beams used in gyrotrons. These considerations could lead in turn to improved design parameters not obtainable by empirical techniques.

The present study represents a numerical extrapolation of the work of Knauer[30] (1966) and Buneman, Levy and Linson[31] (1966) on straight electron beams drifting in crossed electric and magnetic fields. It is anticipated that an increased understanding of these simple cases will allow a similar analysis of beams with continually varying dc parameters. We therefore begin with a derivation of the perturbation equations for the general case, then introduce several simplifications for the present analysis.

4.2 General Equations

The wave motions to be studied here occur in electron beams driven by crossed electric and magnetic fields. In general, the beam will be considered "cold", with no thermal agitation to disturb the uniform drift. The treatment will be non-relativistic, and a quasistatic approach will be used. This is permissible since one finds that the contribution from the self-magnetic field is down by a factor $\frac{v^2}{c^2}$ below the contribution from the applied magnetic or space-charge fields. We therefore have the condition

$$\nabla \times \underset{\sim}{E} = 0 \tag{1}$$

together with Poisson's equation

$$\nabla \cdot \underset{\sim}{E} = \frac{\rho}{\varepsilon_o} \tag{2}$$

an equation of continuity

$$\nabla \cdot \underset{\sim}{j} + \frac{\partial \rho}{\partial t} = 0 \tag{3}$$

and an equation of motion

$$\frac{\partial \underset{\sim}{V}}{\partial t} + (\underset{\sim}{V} \cdot \nabla)\underset{\sim}{V} = -\eta(\underset{\sim}{E} + \underset{\sim}{V} \times \underset{\sim}{B}) \tag{4}$$

where $\eta = \frac{|e|}{m}$. In addition, we note the definition of current density, $\underset{\sim}{j} = \rho \underset{\sim}{V}$ and we introduce the cyclotron frequency $\omega_c = \eta B$.

The coordinate system to be used is shown in Figure 4.1. The general case has a beam emerging from a given area on a cathode into crossed magnetic and electric fields. The magnetic field is into the paper, along the z axis, while the electric field is directed downward, along the -x axis. The beam then rises

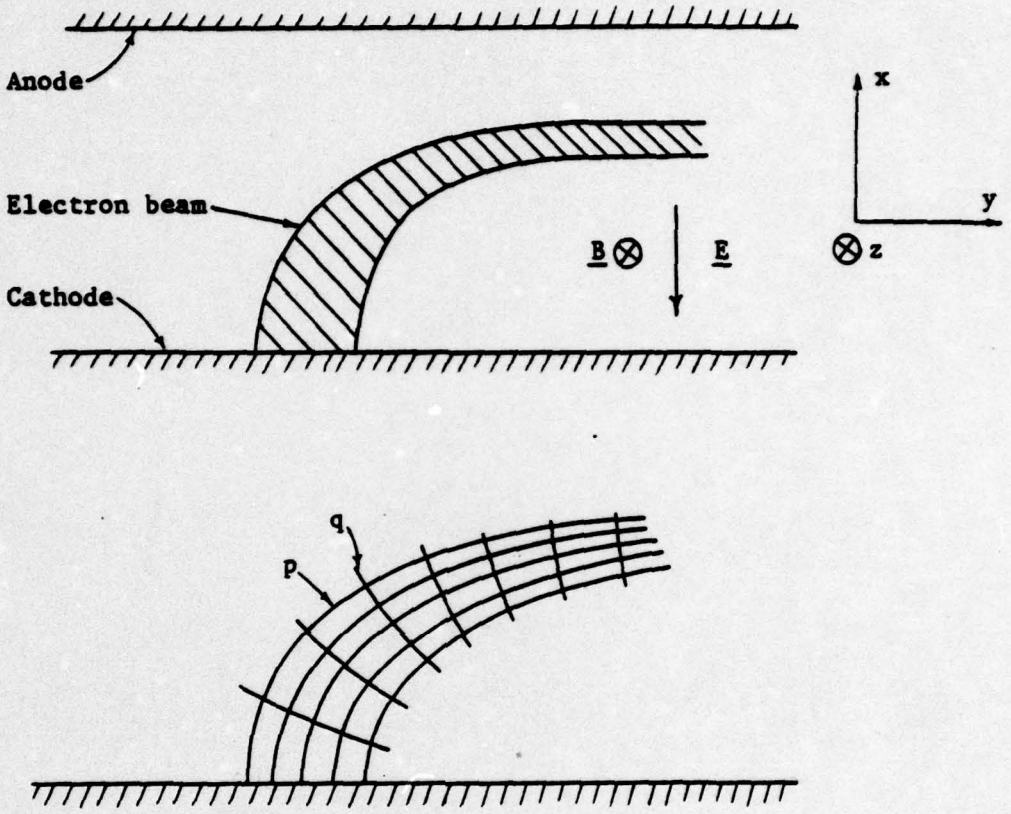

Figure 4.1

Geometry of curving electron beam, showing coordinate systems and orientation of electric and magnetic fields. Note that as the beam bends it turn to the +y direction, with the +x surface on the upper side, the −x surface on the lower.

toward the anode, converging, accelerating and bending to the right, to the +y direction. Hence beam velocity, orientation and density are all changing in this "acceleration" region. The beam then drifts uniformly parallel to the y axis, which is the case to be analyzed in this paper. In order to set up the general equations, however, curvilinear coordinates p along the beam and q across the beam are defined, such that in the drift region q becomes coincident with x, and p with y.

The variables $\underset{\sim}{E}$, $\underset{\sim}{V}$, $\underset{\sim}{j}$ and ρ are split into steady-state and time-varying parts:

$$\underset{\sim}{E} = \underset{\sim o}{E} + \underset{\sim 1}{E} \exp[i(\omega t - kV_{po})] \quad , \text{etc.} \tag{5}$$

Here, V_{po} is the steady-state velocity of the electron beam. The subscripts 1 on perturbed variables will be understood in the following equations. Also, the equations will be written in Cartesian style although curvilinear coordinates would demand scale factors which are not unity. Such scale factors are easily handled numerically but greatly increase the analytical complexity. The equations will therefore be valid for sections of the beam which are small compared to the radius of curvature of the beam.

The following set of five equations then follows for the perturbed quantities:

$$\left(\omega - kV_{po} - i\frac{\partial V_{po}}{\partial p}\right) V_p - iV_{po}\frac{\partial V_p}{\partial p} = iV_q\left(\frac{\partial V_{po}}{\partial q} - \omega_c\right) + i\eta E_p \tag{6}$$

$$(\omega - kV_{po})V_q - iV_{po}\frac{\partial V_q}{\partial p} = i\omega_c V_p + i\eta E_q \tag{7}$$

$$\left(\omega - kV_{po} - i\frac{\partial V_{po}}{\partial p}\right)\rho - iV_{po}\frac{\partial \rho}{\partial p} = k\rho_o V_p + i\frac{\partial}{\partial p}(\rho_o V_p) + i\frac{\partial}{\partial q}(\rho_o V_q) \tag{8}$$

$$\frac{\partial E_p}{\partial q} + ikE_q = 0 \tag{9}$$

$$\frac{\partial E_q}{\partial q} - ikE_p = \frac{\rho}{\varepsilon_o} \tag{10}$$

At this point it is possible to solve the equations for any one quantity, such as E_p or E_q, or an electrostatic potential ϕ. Both Gould[29] and Knauer[30] solved for E_p. However, Buneman et al[31] found that solving for V_q was most fruitful, since various analytical difficulties were thereby avoided. For example, this makes the equations immediately compatible with the boundary conditions, which are formulated most easily in terms of V_q.

4.3 Formulation for Straight Beams

In order to reduce the five equations to a single one in V_q, for a straight beam, it will be implicitly assumed that the perturbation amplitudes do not grow along the beam. Convection terms, that is, terms involving p derivatives, will therefore be dropped, although this does not rule out the possibility of growth rates appearing as complex k. Density ρ_o will be assumed constant and also the velocity shear will be taken constant:

$$\frac{\partial V_{po}}{\partial q} = \omega_s \tag{11}$$

Finally, because we are analyzing a beam in the drift region of tube, subscripts p will be changed to y, q to x.

The equations then become:

$$(\omega - kV_{yo})V_y = iV_x(\omega_s - \omega_c) + i\eta E_y \tag{12}$$

$$(\omega - kV_{yo})V_x = i\omega_c V_y + i\eta E_x \tag{13}$$

$$(\omega - kV_{yo})\rho = k\rho_o V_y + i\rho_o \frac{\partial V_x}{\partial x} \tag{14}$$

$$\frac{\partial E_y}{\partial x} + ikE_x = 0 \tag{15}$$

$$\frac{\partial E_x}{\partial x} - ikE_y = \frac{\rho}{\varepsilon_o} \tag{16}$$

Following Buneman et al, we substitute E_y, E_x and ρ from the first three equations into the last two, obtaining

$$[i(\omega - kV_{yo})V_y + (\omega_s - \omega_c)V_x]' = -ik[i(\omega - kV_{yo})V_x + \omega_c V_y] \tag{17}$$

$$[i(\omega - kV_{yo})V_x + \omega_c V_y]' - ik[i(\omega - kV_{yo})V_y + (\omega_s - \omega_c)V_x] = -\frac{\omega_p^2 (V_x' - ikV_y)}{i(\omega - kV_{yo})} \quad (18)$$

where $\omega_p^2 = -\frac{\eta\rho_o}{\varepsilon_o}$ is the square of the plasma frequency and primes denote differentiation with respect to x. The derivatives are taken inside the brackets and V_y' is eliminated by multiplying the first equation by ω_c, the second, by $i(\omega - kV_{yo})$, and subtracting. This yields

$$ikV_y = V_x' + \frac{2k\omega_s(\omega - kV_{yo})}{\Omega^2} V_x \quad (19)$$

where

$$\Omega^2 = \omega_c^2 - (\omega - kV_{yo})^2 - (\omega_c\omega_s - \omega_p^2) \quad (20)$$

Substituting this expression for V_y back into the first equation, one finds

$$\left[V_x' + \frac{2k\omega_s(\omega - kV_{yo})}{\Omega^2} V_x\right]' = k^2 V_x\left[1 + \frac{2\omega_s(\omega_s - \omega_c)}{\Omega^2}\right] \quad (21)$$

This equation may be rendered in the form

$$\frac{\partial^2 V_x}{\partial x^2} + r(k,\omega)\frac{\partial V_x}{\partial x} + s^2(k,\omega)V_x = 0 \quad (22)$$

where

$$r(k,\omega) = \frac{2k\omega_s(\omega - kV_{yo})}{\Omega^2}$$

$$s^2(k,\omega) = -\frac{2k^2\omega_s^2}{\Omega^2}\left[1 + \frac{2(\omega - kV_{yo})^2}{\Omega^2}\right] + \frac{2k^2\omega_s(\omega_c - \omega_s)}{\Omega^2} - k^2 \quad (23)$$

4.4 Boundary Conditions

The surface of the beam is undulating because of perturbing surface waves. However, its effect can be well approximated by treating undulations as variations in surface charge density of a rigid-sided beam. This is known as the "mean surface approximation". Conservation of charge flow in the boundary layer is expressed by the equation

$$\frac{\partial \sigma}{\partial t} = \pm j_x - V_{yo} \frac{\partial \sigma}{\partial y} \tag{24}$$

where the upper sign refers to the +x side of the beam, the lower sign, to the -x side; σ is the surface charge. Taking σ to vary as $\exp[i(\omega t - ky)]$ one finds

$$\sigma = \frac{\mp j_x}{i(\omega - kV_{yo})} \tag{25}$$

Across such a surface, internal and external fields match according to the relations

$$E_{y1} = E_{y2} \tag{26a}$$

$$E_{x1} = E_{x2} \pm \frac{\sigma}{\varepsilon_o} \tag{26b}$$

where subscripts 1 and 2 denote fields inside and outside the beam, respectively. Anticipating that the electrical potential will decay with distance from the beam, we may set

$$\phi = (\phi^+ e^{kx} + \phi^- e^{-kx}) \exp[i(\omega t - ky)] \tag{27}$$

hence

$$E_{y_2} = ik(\phi^+ e^{kx} + \phi^- e^{-kx}) \exp[i(\omega t - ky)] \tag{28}$$

$$E_{x_2} = -k(\phi^+ e^{kx} - \phi^- e^{-kx}) \exp[i(\omega t - ky)] \tag{29}$$

Therefore the following combinations are appropriate to the +x and -x sides of the beam, respectively:

$$E_{x_2} - i E_{y_2} \propto \phi^- e^{-kx} \tag{30a}$$

$$E_{x_2} + i E_{y_2} \propto \phi^+ e^{kx} \tag{30b}$$

In order for the solution (30b) not to exist on the +x side away from the beam, we set $\phi^+ = 0$ or

$$E_{x_2} + i E_{y_2} = 0 \tag{31a}$$

Similarly, for the solution (30a) not to exist on the -x side away from the beam, we set $\phi^- = 0$ or

$$E_{x_2} - i E_{y_2} = 0 \tag{31b}$$

Inserting these relations into the second boundary condition, equation (26b), and substituting for σ,

$$E_{x_1} = \mp i E_{y_2} - \frac{j_x}{i \varepsilon_o (\omega - k V_{yo})} \tag{32}$$

From the first boundary condition (26a), $E_{y_2} = E_{y_1}$ and the x and y components of the internal electric field at the beam edge are related by

$$E_{x_1} = \mp i E_{y_1} - \frac{j_x}{i \varepsilon_o (\omega - k V_{yo})} \tag{33}$$

Substituting first for E_x and E_y from the equations of motion, (12) and (13), then for V_y from (19), the boundary condition becomes

$$\frac{\partial V_x}{\partial x} + a_\pm V_x = 0 \tag{34}$$

where

$$a_\pm (k,\omega) = k \left[\frac{2\omega_s (\omega - k V_{yo})}{\Omega^2} + \frac{\omega_p^2 \mp \omega_s (\omega - k V_{yo})}{(\omega - k V_{yo}) [\omega_c \mp (\omega - k V_{yo})]} \pm 1 \right] \tag{35}$$

4.5 Solution Scheme

An eigenvalue technique was used to solve equation (22) together with the boundary condition (34). This was done in two ways, one to find complex ω given real k, the other to find complex k given real ω. The eigenvalue formulation for ω versus real k is produced by multiplying equation (22) by $\frac{\Omega^2}{\omega^2}$.

$$\frac{\Omega^2}{\omega^2}\frac{\partial^2 V}{\partial x^2} + r'\frac{\partial V}{\partial x} + s'^2 V = \lambda^2 V \tag{36}$$

where

$$r' = \frac{2k\omega_s(\omega - kV_{yo})}{\omega^2} \tag{37}$$

$$s'^2 = -\frac{2k^2\omega_s^2}{\omega^2}\frac{2(\omega - kV_{yo})^2}{\Omega^2} + \frac{2k^2\omega_s(\omega_c - \omega_s)}{\omega^2} - \frac{k^2\Omega^2}{\omega^2} \tag{38}$$

$$\lambda^2 = \frac{2k^2\omega_s^2}{\omega^2} \tag{39}$$

Here, V_x has been replaced by V. Central difference terms are substituted for the derivatives to give an equation in discrete V_j, $j = 1,\ldots, N$

$$\left(\frac{\Omega^2}{\omega^2} - \frac{1}{2}r'h\right)V_{j-1} + \left(\frac{-2\Omega^2}{\omega^2} + s'^2h^2\right)V_j + \left(\frac{\Omega^2}{\omega^2} + \frac{1}{2}r'h\right)V_{j+1} = h^2\lambda^2 V_j \tag{40}$$

N-2 equations are possible for N points across the beam, with spacing h between points. Subscript 1 represents the -x edge of the beam, subscript N, the +x edge of the beam. The boundary conditions (34) at these edges can be formed by Taylor expansion about the end points (Abramowitz and Segun[35], formula 25.3.4 with p = 1) to produce the formulas

$$\frac{3V_1 - 4V_2 + V_3}{2h} - a_- V_1 = 0 \qquad -x \text{ edge} \tag{41}$$

$$\frac{3V_N - 4V_{N-1} + V_{N-2}}{2h} + a_+ V_N = 0 \qquad +x \text{ edge} \tag{42}$$

By adding $\lambda^2 V_1$ and $\lambda^2 V_N$ to each side of the respective boundary conditions, sufficient equations are available to form an N x N matrix $\underline{\underline{M}}$, such that

$$\underline{\underline{M}}\underline{V} = \lambda^2 \underline{V} \tag{43}$$

Since $\underline{\underline{M}} = \underline{\underline{M}}(\lambda^2)$, an initial value may be chosen for λ^2, then a self-consistent value found by the formulation

$$\underline{\underline{M}}(\lambda^2_{i-1})\underline{V} = \lambda^2_i \underline{V} \tag{44}$$

where eventually the difference between λ_{i-1} and λ_i is expected to be less than some small quantity ε.

In practice, however, convergence can be slow by this iterative technique. It was found more effective to define a complex difference function

$$d_{i-1} = \omega_i - \omega_{i-1} \tag{45}$$

where ω_{i-1} is a trial value of ω used to produce λ_{i-1}, which in turn produces λ_i by equation (44), hence ω_i by (39). Zeroes of the function d_{i-1} are located by various standard techniuqes, the most efficient being to bracket the zero by searching over ω_{i-1} space, then to locate it rapidly by quadratic interpolation.

The eigenvalue formulation for k vs. real ω is produced directly from equation (22):

$$\frac{\partial^2 V}{\partial x^2} + r'' \frac{\partial V}{\partial x} + s''^2 V = \lambda^2 V \tag{46}$$

where $r'' = r$ and

$$s''^2 = -\frac{2k^2\omega_s^2}{\Omega^2}\left[1 + \frac{2(\omega - kv_{yo})^2}{\Omega^2}\right] + \frac{2k^2\omega_s(\omega_c - \omega_s)}{\Omega^2} \tag{47}$$

$$\lambda^2 = k^2 \tag{48}$$

The difference equation is

$$(1 - \tfrac{1}{2} r''h)V_{j-1} + (-2 + s''^2h^2)V_j + (1 + \tfrac{1}{2} r''h)V_{j+1} = h^2\lambda^2 V_j \tag{49}$$

and the boundary conditions are as before.

In the numerical work presented here, eleven equally-spaced points were used across the beam, with nine on the interior and two on the edges. In all cases a close match was found between numerically derived curves and parts of previous analytical curves. No significant improvement was found when the number of points across the beam was increased. This is because the fundamental mode and the first harmonic, adequately described by 11 points, were the principal sources of information for the various curves.

4.6 Beam with No Velocity Shear

We begin our analysis by examining a uniform electron beam of finite width 2a drifting in crossed electric and magnetic fields. Following Knauer[30] we shall treat the case of zero velocity shear across the beam. We begin with equation (36), setting $\omega_s = 0$ in the terms r' and s' to obtain $r' = 0$, $s'^2 = -k^2\Omega^2/\omega^2$, and hence

$$\frac{\Omega^2}{\omega^2}\left(\frac{\partial^2 V}{\partial x^2} - k^2 V\right) = 0 \tag{50}$$

Several solutions follow from this equation. Setting $\Omega^2 = 0$, we have the dispersion relation

$$(\omega - kV_{yo})^2 = \omega_c^2 + \omega_p^2 \tag{51}$$

According to Knauer, this relation comprises various oscillations and waves confined to the interior of the beam. These modes will not be treated here. Other modes which increase towards the surface inside the beam are given by

$$\frac{\partial^2 V}{\partial x^2} - k^2 V = 0 \tag{52}$$

Solutions to this equation are of the form $V = c_1 e^{\pm kx}$. Because equation (52) is a free space field equation, the charge density within the beam remains undisturbed. The resulting waves are then surface waves, and the solution $V = c_1 e^{kx}$ is appropriate to the +x edge, while the solution $V = c_1 e^{-kx}$ is appropriate to the -x edge. Inserting these solutions into the respective boundary conditions, we have

$$\pm k e^{\pm kx} + k\left[\frac{\omega_p^2}{(\omega - kV_{yo})[\omega_c \mp (\omega - kV_{yo})]} \pm 1\right] e^{\pm kx} = 0 \tag{53}$$

This simplifies to

$$\omega_p^2 = \mp 2(\omega - kV_{yo})[\omega_c \mp (\omega - kV_{yo})] \tag{54}$$

Setting $u = \omega - kV_{yo}$, solutions are given by

$$u_1 = +\frac{1}{2}\omega_c \pm \frac{1}{2}\sqrt{\omega_c^2 + 2\omega_p^2}$$

$$u_2 = -\frac{1}{2}\omega_c \pm \frac{1}{2}\sqrt{\omega_c^2 + 2\omega_p^2} \tag{55}$$

The corresponding curves of $\frac{\omega}{\omega_c}$ versus ka are shown in Figure 4.2 where $\frac{\omega_p^2}{\omega_c^2} = 0.5$, and the normalized velocity $V_{yo}/\omega_c a = 0.5$. Figure 4.3 shows the same curves on log-log scale for comparison with later diagrams. In practical terms, the curves may correspond to a magnetic field of 114 gauss, ω_c = 2 GHz cyclotron frequency, a beam width of 0.1 mm and a beam velocity $V_{yo} \simeq 10^5$ m/sec.

The four curves were confirmed using the same computer program used later to develop more complicated dispersion curves. The curves of Figures 4.2 and 4.3 are symmetrically placed about the line $\omega = kV_{yo}$ (called the "synchronous axis"). The modes above the synchronous axis are propagating faster than the beam velocity, while those below are propagating slower. Relative to the moving beam, the curves closer to the synchronous axis may be considered "slow" modes, while those farther away are "fast" modes. Knauer describes the particle motion in the slow mode as circular, with electrical and magnetic forces opposing, while the fast mode consists of circular particle motion in which electrical and magnetic forces are aligned. When a velocity slip is present, interaction between the slow waves of the two surfaces of the beam gives rise to the diocotron, or slipping stream instability.

Also marked on the diagram are the eigenvectors which correspond to the various curves. As described in the solution to equation (52), surface waves for

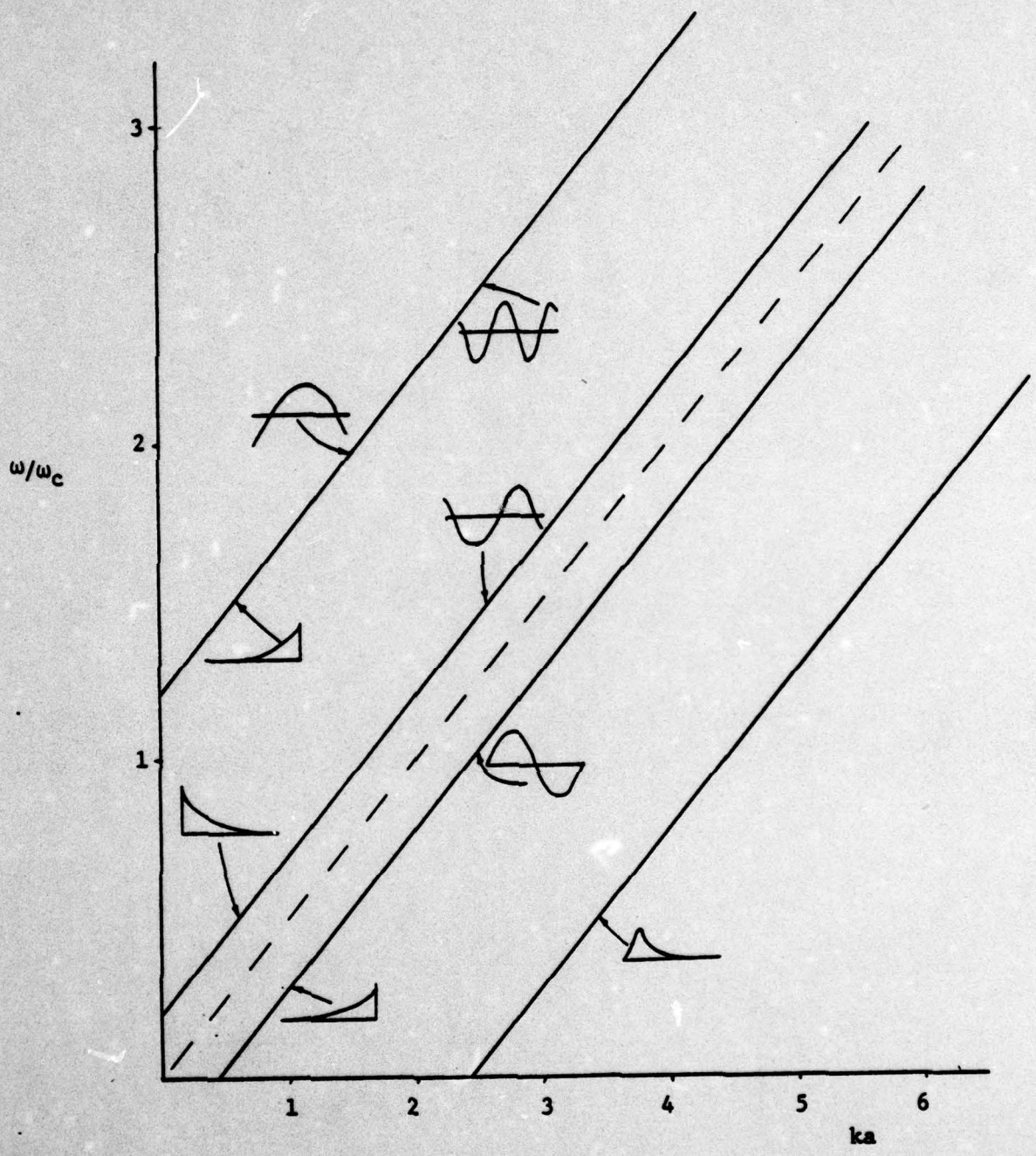

Figure 4.2

Dispersion curves for various modes of oscillation in a drifting electron beam with no velocity shear. $\omega_p^2/\omega_c^2 = 0.5$. Velocity distributions for the modes are sketched near curves.

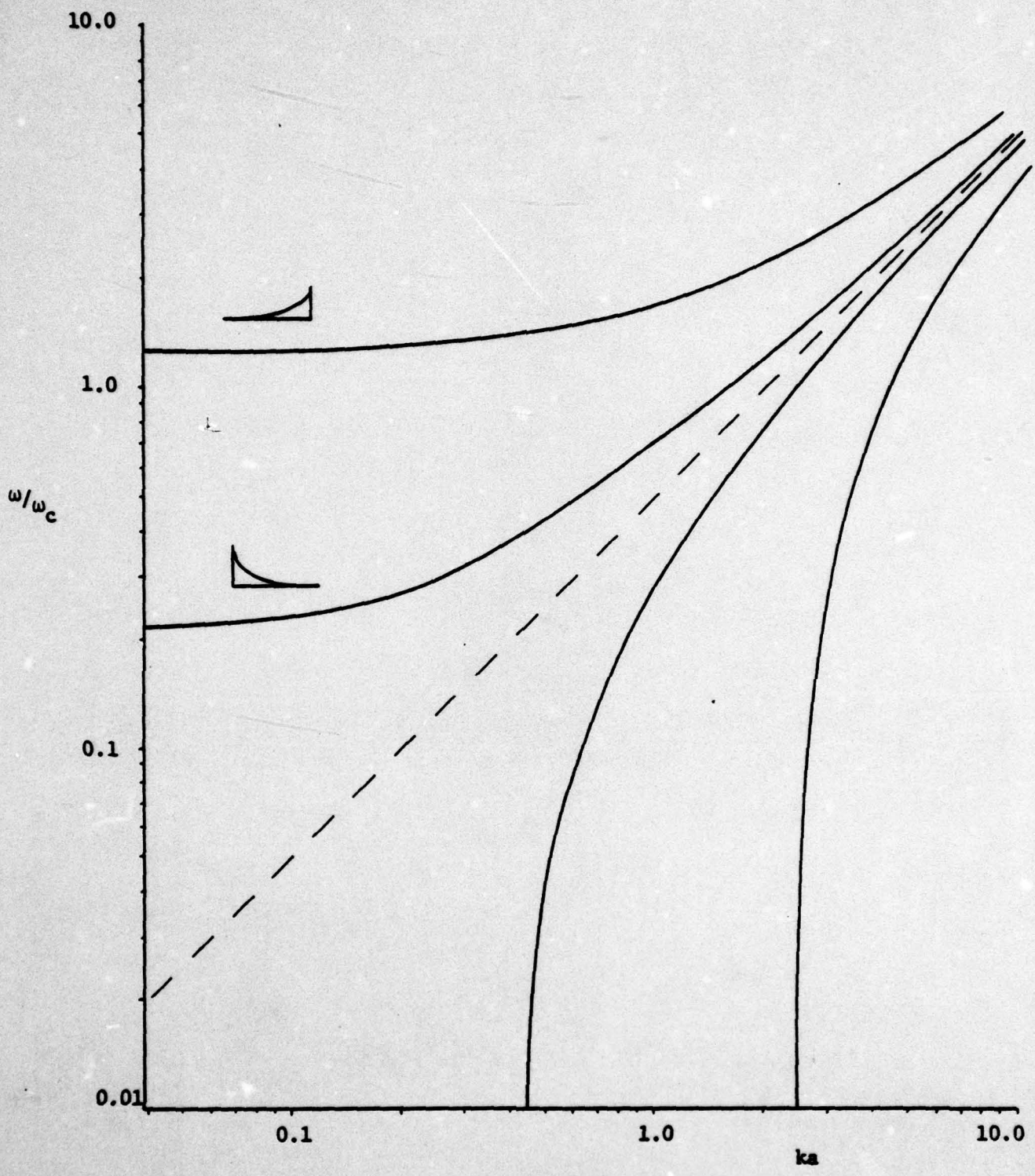

Figure 4.3

Dispersion curves as in Figure 4.2 on log-log scale. Those curves above the line $\omega = kV_{yo}$ represent waves travelling faster than the beam velocity, those below the line, waves slower than beam velocity.

$ka \ll 1$ are functions which decrease exponentially from the surface into the beam. For higher ka, various types of internal perturbation are evident.

4.7 Beam with Velocity Shear, No Drift

For long wavelength instabilities, ka << 1, the flow may be considered incompressible. Qualitatively, this is related to the tendency of particles under such perturbations to behave as they do in equilibrium, and drift at the E/B velocity. $\underset{\sim}{E}$ - field perturbations are then divergenceless as well as curl-free, and so are the velocity perturbations (being the $\underset{\sim}{E}$ pattern turned through 90° The two boundaries, however, undulate under the perturbing field, and represent surface-charge waves that communicate with each other across the apparently "empty" space between them. For a convenient description of this interaction, one may choose a frame of reference in which the centre of the beam is at rest. Since this frame is symmetrical with respect to the two interacting surface waves, the resultant growing wave mode can be expected to be stationary. Its variation in time and space is then expressible as exp (iωt - iky) where ω is pure imaginary, representing the growth rate.

For the case $\omega_s = 0$, no imaginary solution for ω is expected since equations (55) do not permit such a solution. Buneman et al[31] has treated the case $\omega_s \neq 0$ for the special circumstance $\omega_s\omega_c = \omega_p^2$. This relation follows from the dc electrostatic fields set up by the presence of the drifting electrons. Such fields are directed inward toward the beam, in the x-direction, according to the relation

$$\frac{dE'}{dx} = \frac{\rho_o}{\varepsilon_o} \tag{56}$$

where $\rho_o < 0$ is the charge density of the electron beam. Under the influence of this secondary E' field and the ambient magnetic field, the electrons drift with a velocity -E'/B. The velocity shear is then given by

$$\omega_s = \frac{dV}{dx} = -\frac{d}{dx}\left(\frac{E'}{B}\right) = -\frac{\rho_o}{\varepsilon_o B} = \frac{\omega_p^2}{\omega_c} \tag{57}$$

Buneman's results are shown in Figure 4.4. The velocity shear is $\omega_s = 0.5\omega_c$ in this case (i.e. $\beta = 0.5$). The pure imaginary curve is apparent for low ka. As ka increases from these values, the two interacting surface waves become further removed from each other and growth rate diminishes. This is a consequence of the incompressible nature of the beam interior: since electric fields are derivable from a potential that solves Laplace's equation, and since variations are sinusoidal in the y direction, the time and space variation must be of the form

$$\phi \sim e^{\pm kx} \exp[i(\omega t - ky)] \tag{58}$$

This exponential behaviour in the x direction was alluded to earlier. Lord Rayleigh's derivation of the $ka \ll 1$ situation shows that above $ka = 0.64$ the instability becomes stable and that a real solution exists (eg. Hasegawa[36]). Buneman's long wavelength derivation for general $\beta = \frac{\omega_s}{\omega_c} < 1$ shows a transition from instability to stability at ka given by

$$ka = 0.64 + 0.32\beta + 0.02\beta^2 \tag{59}$$

or $ka = 0.805$ in our case ($\beta = 0.5$). The maximum growth rate for $ka \ll 1$ is given by

$$\mathrm{Im}\frac{\omega}{\omega_c} = 0.20\beta + 0.1\beta - 0.04\beta^2 \tag{60}$$

For intermediate wavelengths no unstable waves are present. For short wavelengths, above ka given by

$$ka = 0.5\beta^{-1} + 0.25 + 0.125\beta - 0.11\beta^2 \tag{61}$$

or $ka = 1.285$ in our case, growing waves are again present. The instability is due to resonance at the gyrofrequency between a surface wave and a compressive

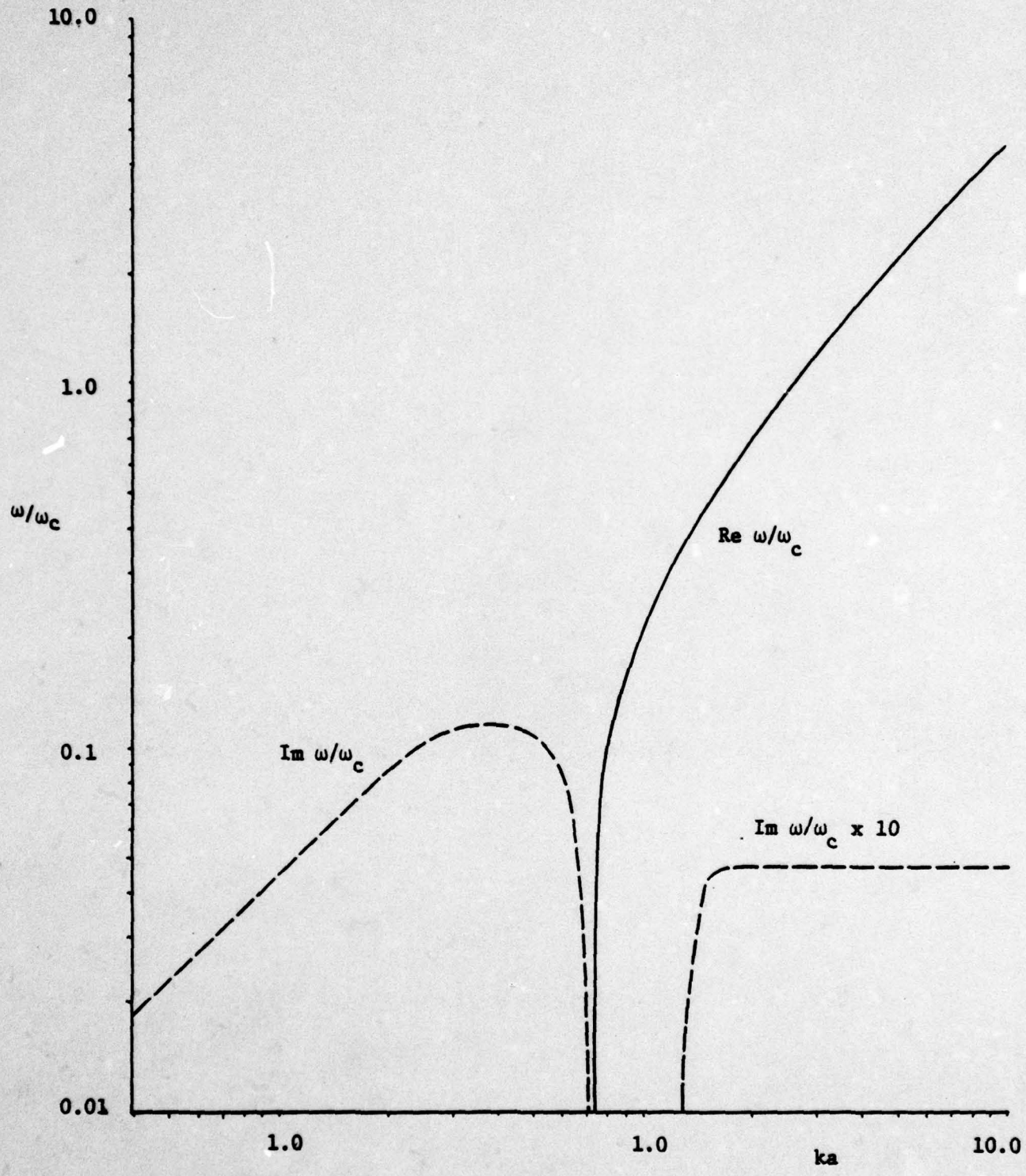

Figure 4.4

Dispersion curves derived analytically by Buneman, Levy and Linson[31] for a stationary beam with velocity shear $\omega_s = 0.5\ \omega_c$. As in Figure 4.2, $\omega_p^2/\omega_c^2 = 0.5$. The real ω curve is shown as a solid line, the pure imaginary ω curves, as dashed lines. Note, the rightmost imaginary ω is a factor of 10 less than shown here.

wave within the beam. At these wavelengths, the previous assumption of an incompressible beam is no longer valid. The short wavelength instability occurs for beams wide relative to the wavelength (specifically, for which $k(2a)\omega_s > \omega_c$ is true). The surface wave propagates without strong coupling to any other wave; it sees small reflections from the gyro-resonant layer through a substantial width of almost transparent beam. The dispersion relation for this mode is given by

$$\frac{\omega}{\omega_c} = [ka\beta - 0.5\beta - 0.25\beta^2] + i\left(\frac{\pi\beta}{2e}\right) e^{-2/\beta} \qquad (62)$$

The real and imaginary parts are shown in Figure 4.4.

4.8 Numerical Analysis of Beam with Velocity Shear, No Drift

Dispersion curves were developed numerically, as described in section 4.5, for the case $V_{yo} = 0$ at beam centre but $\omega_s \neq 0$. The curves are shown in Figure 4.5. They are similar in several ways to Buneman's curves, Figure 4.4, with the one striking difference that the real curve of Figure 4.4 has been crossed by a second real curve running approximately linearly from $\omega = \omega_c$ on the ω axis to $ka = 1.45$ on the k axis. The crossover occurs at the $ka = 1.12$, and has resulted in the division of the two curves into an upper branch and a lower branch. Figure 4.6 shows the dispersion curves in a linear plot.

Among the many similarities, the imaginary ω curves below $ka = 0.77$ are identical, as are the corresponding real dispersion curves away from the cross-over point. To the right of the lower branch, a complex curve occurs in Figure 4.5 which has a corresponding complex curve in Figure 4.4. The continuation of this latter curve is not certain, as the points were difficult to locate beyond $ka = 1.8$. The imaginary curve is shown, with the real parts being less by a factor 0.01. Three points on this curve are given in the following table:

ka	ω/ω_c
1.6	(0.000115, 0.05670)
1.7	(0.00112, 0.0900)
1.8	(0.00231, 0.0941)

In Buneman's analysis an asymptotic value of 0.005 was given for the imaginary part of $\frac{\omega}{\omega_c}$ at $\beta = 0.5$, for large ka. The present analysis suggests a larger growth rate for gyro-resonance conditions in straight electron beams. This may be related to the high gain observed in gyrotrons. In addition, the real parts are less than in Buneman's formula, equation (62). That equation implies, in

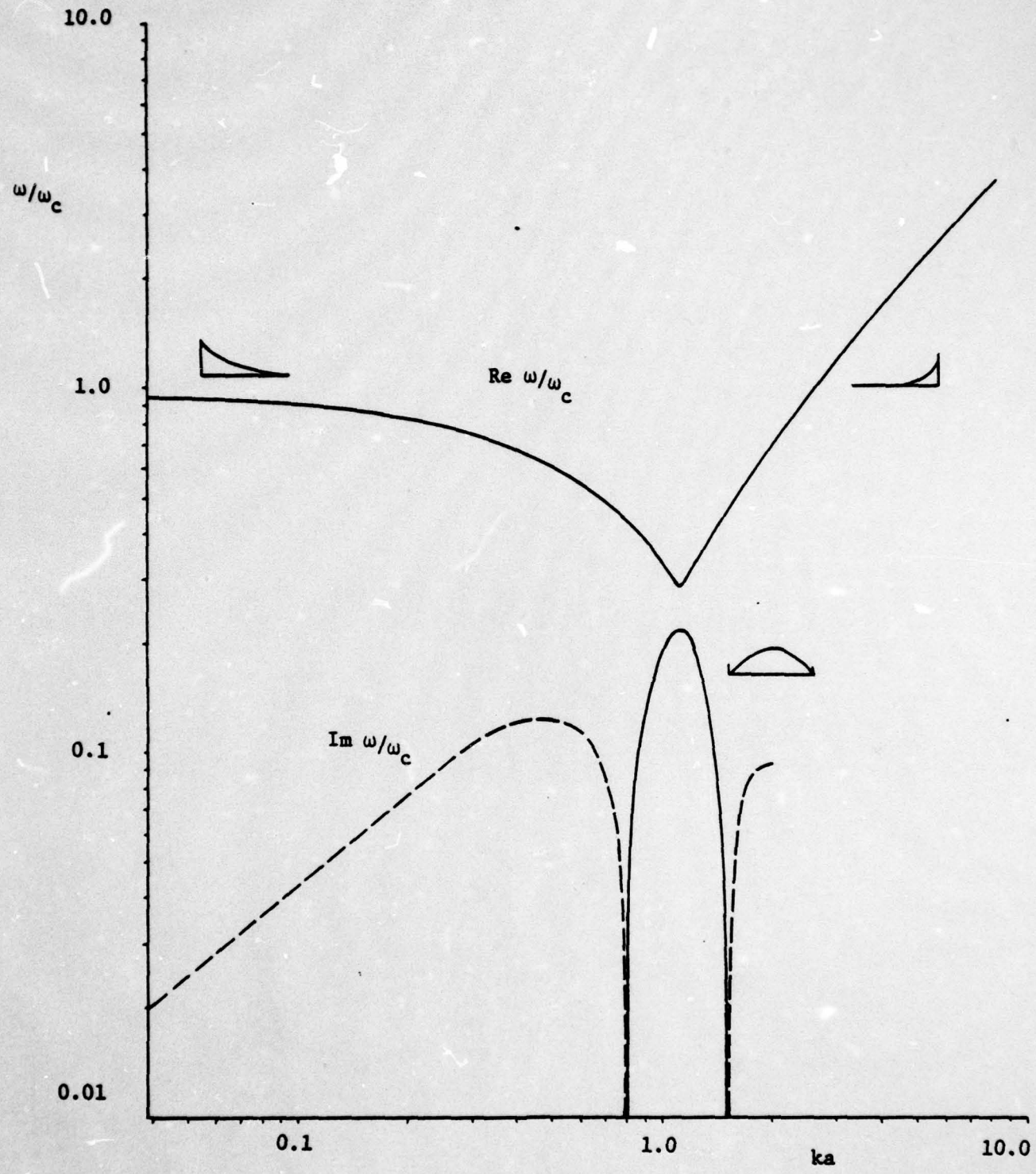

Figure 4.5

Dispersion curves derived numerically, using the same parameters as in Figure 4.4(stationary beam with velocity shear $\omega_s = 0.5\ \omega_c$). Real ω curves, corresponding to stable waves, as shown as solid lines, while imaginary curves, corresponding to growing modes stationary in the rest frame of the beam, are shown as dashed lines.

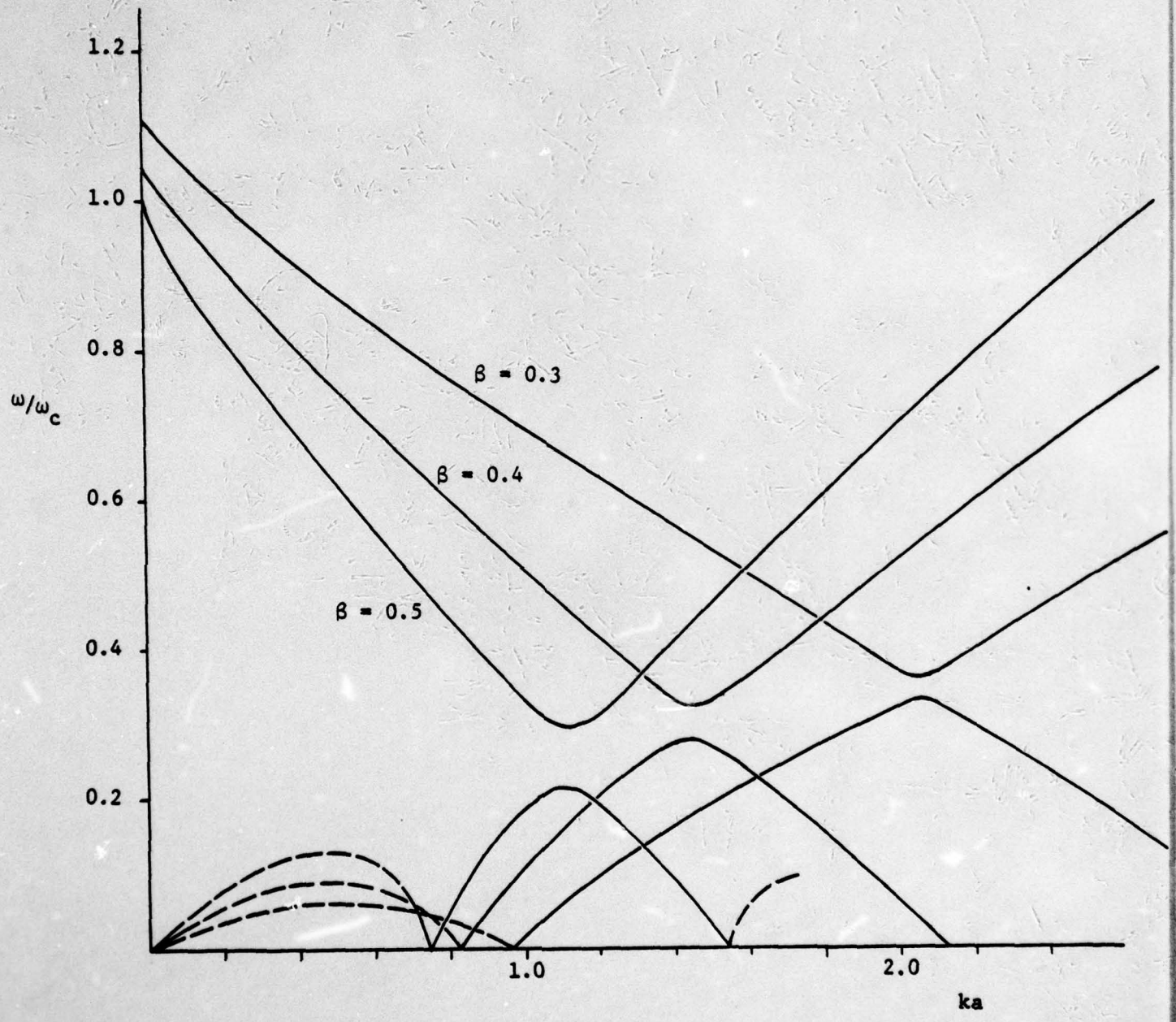

Figure 4.6

Dispersion curves for a sationary beam with velocity shear $\omega_s = \beta\omega_c$. Curves are shown for $\beta = 0.3, 0.4$ and 0.5. The dashed lines represent imaginary ω, to which the corresponding real part is a fraction 0.01 or less. Note the tendency to higher ka as β decreases.

fact, that the real part is none other than the real branch of the dispersion curve, Figure 4.4. No such complex solution was found in our analysis. Another difference, a minor one, is that the point of commencement of our complex curve is at ka = 1.45, rather than the value ka = 1.285 given by Buneman et al (equation (61)).

The physical meaning of the real dispersion curves in Figures 4.5 and 4.6 can be found from an examination of the associated eigenvectors. These are shown in Figures 4.7 and 4.8 for various points along the curves. Small sketches of these are also shown in Figure 4.5. The upper branch is apparently a surface wave mode, while the lower branch is a bulk wave mode. As ka increases, the relative depth of penetration of the surface wave into the beam interior decreases. Note that in the reference frame in which the centre of the beam is at rest all waves are propagating in the +y direction, but the electrons on the -x side are moving in the -y direction while those on the +x side are moving in the +y direction.

The two intersecting dispersion curves may be related to the "slow" and "fast" waves of Figure 4.3, where velocity shear is absent. Figure 4.6 shows the curves of Figure 4.5 on linear scale, for $\beta = 0.5$, 0.4 and 0.3. As β decreases, it appears that the dispersion curve which forms the left half of the upper branch and the right half of the lower branch is shifting to higher ka. In fact, it appears to be rotating about some point just to the left of the ω axis. The other dispersion curve is likewise turning toward the k axis. By an extrapolation of this trend one could imagine a mapping into the fast and slow curves, respectively, of Figure 4.3.

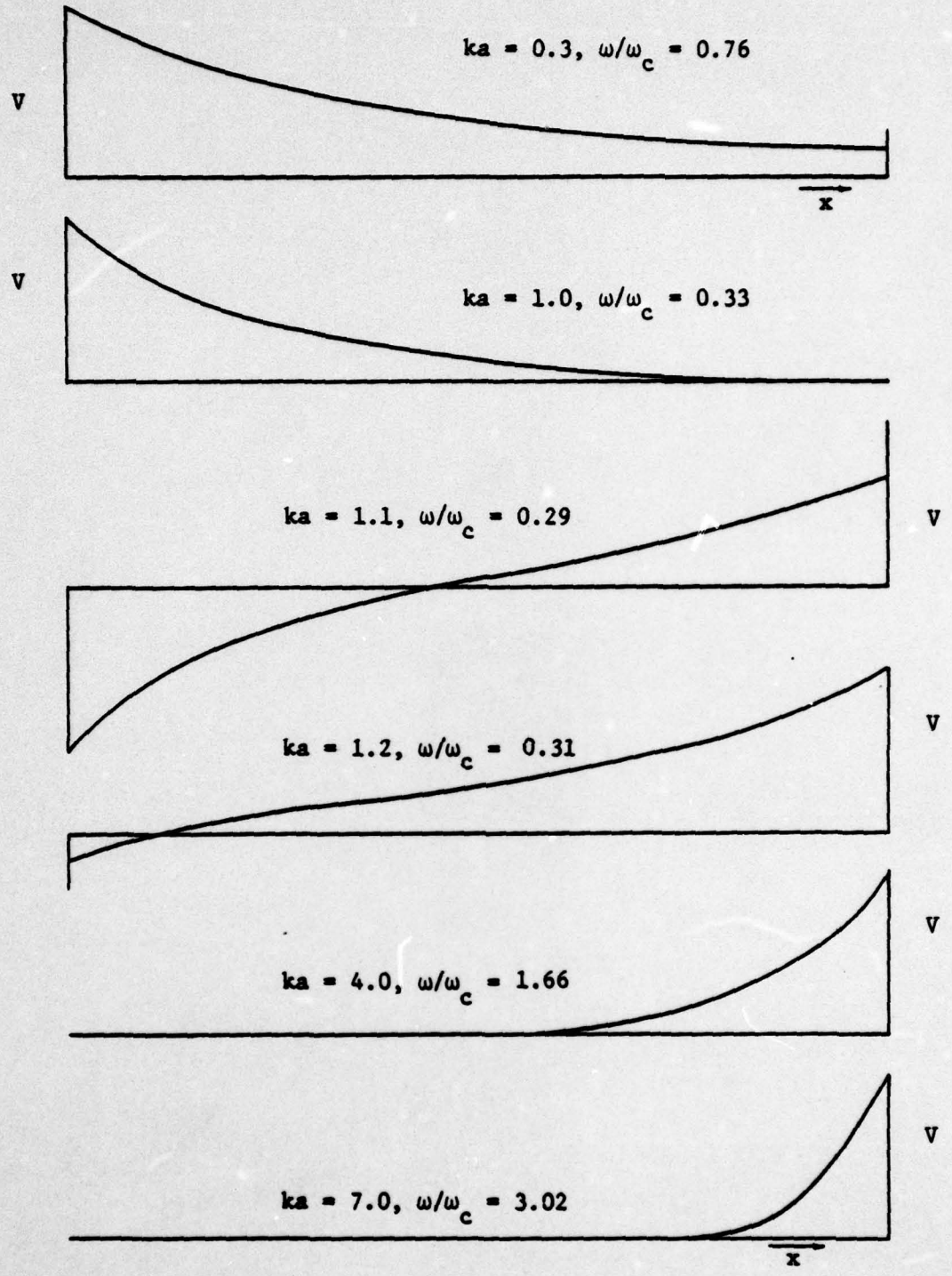

Figure 4.7

Velocity distributions across the beam for a succession of points along the upper branch of the real dispersion curve, Figure 4.5. As ka increases, these show a transition from a surface wave on the -x surface to one of the +x surface

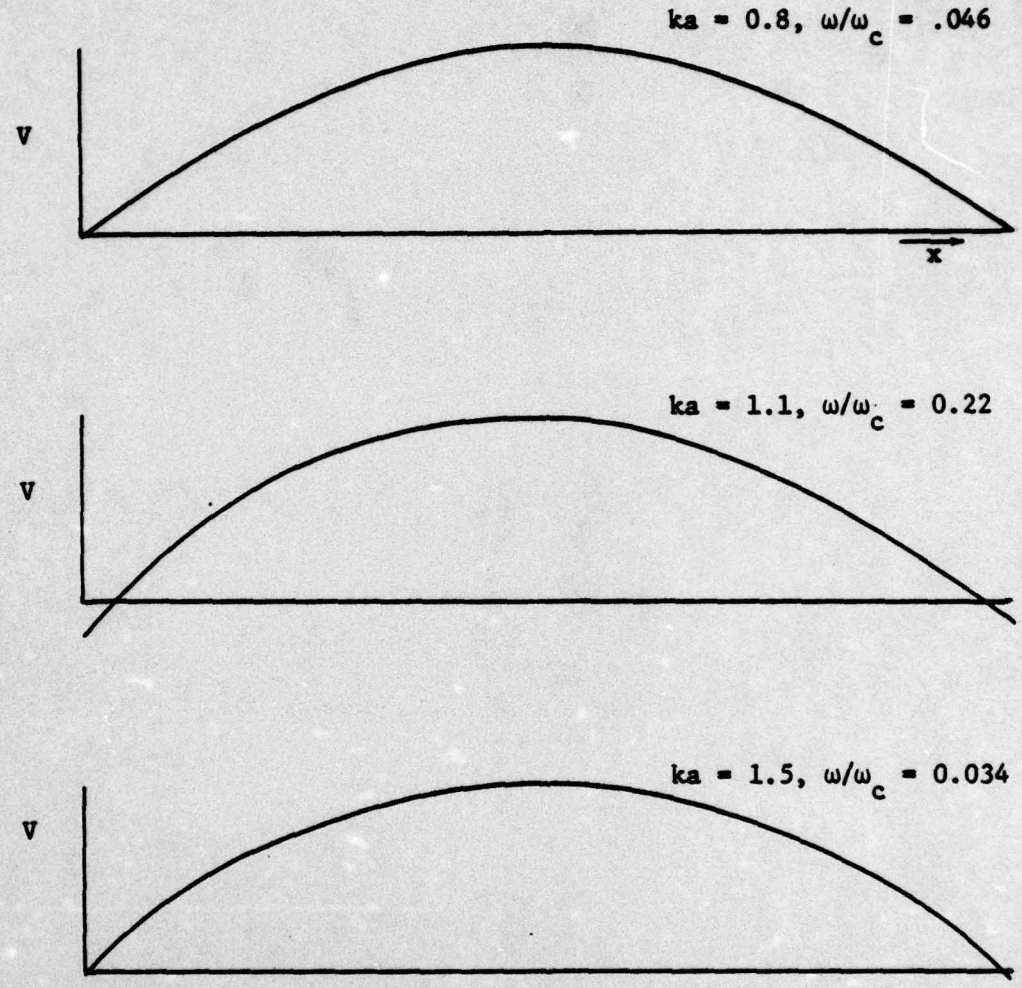

Figure 4.8

Velocity distributions across the beam for a succession of points along the lower branch of the real dispersion curve, Figure 4.5. These represent bulk compressional waves on the beam interior (the velocity peaks shown here being the amplitude of waves propagating along the beam with wavenumber k, velocity ω/k).

The dependence of several curve parameters on β can be ascertained from Figure 4.6. Consider the changeover point from unstable to stable waves, given by equation (59). The point has been worked out for three values of β. The following table gives a comparison between previous analytical values and values numerically derived in the present analysis:

	ka	
β	analytical	numerical
0.3	0.738	0.98
0.4	0.771	0.83
0.5	0.805	0.76

We found that the changeover point moved to lower ka with increasing β, contrary to Buneman's findings.

The maximum growth rate for ka << 1 is given by equation (60). The following β dependences were found:

	max Im ω/ω_c	
β	analytical	numerical
0.3	0.113	0.063
0.4	0.117	0.084
0.5	0.120	0.123

Our results, while being more strongly dependent on β, show a trend to increasing Im ω/ω_c with increasing β.

The onset of growing waves in the gyroresonance regime is given analytically by equation (61). The following β dependences were found:

	ka	
β	analytical	numerical
0.3	1.944	3.09
0.4	1.532	2.10
0.5	1.285	1.55

Again, the behaviour with β of the two results is similar.

The slope of the real curve is given by the first derivative of equation (62) with respect to ka. This is simply β. The following values were found:

	slope $\frac{d(\omega/\omega_c)}{d(ka)}$	
β	analytical	numerical for $\omega/\omega_c = 0.1$
0.3	0.300	0.30
0.4	0.400	0.38
0.5	0.500	0.50

The agreement here is very close. The only strong disagreement, then, between previous analytical and present numerical results is the dependence with β of the changeover between unstable and stable waves in the region $ka < 1$.

4.9 Beam with Drift and Velocity Shear

The cases presented in the last two sections may be combined to produce a picture of the behaviour of a drifting beam with velocity shear. Recall that the beam is "cold", with electrons drifting parallel to the beam axis. In section 4.8 the beam centre was taken to be stationary. A pure imaginary ω was found for $ka \ll 1$; this means that a growing wave mode is stationary in the rest frame of the beam. This follows from the symmetry of the oppositely directed electron streams about the beam centre. In a moving beam, therefore, one would expect $\omega = kV_{yo}$ to be added to the real part of this and all other dispersion curves.

In section 4.7 the beam was taken to be uniformly drifting. This resulted in dispersion curves which were symmetrically placed about $\omega = kV_{yo}$. By analogy, one might expect similar behaviour when velocity shear is combined with beam drift.

Figure 4.9 shows the real parts of the dispersion curves for $\beta = 0.5$, and $\frac{V_{yo}}{\omega_c a} = 0.5$, derived numerically as in the previous figures. As expected, $\omega = kV_{yo}$ has been added to the real part of all curves; also, a second set of curves appears which are vertically symmetrical about the line $\omega = kV_{yo}$. In the region $ka < 0.65$ the two real curves coalesce to form a curve along the $\omega = kV_{yo}$ axis; the imaginary part of this curve is precisely as in Figure 4.5. (It is coincidental that the $\omega = kV_{yo}$ curve is asymptotic to the Im ω curve, since both β and $\frac{V_{yo}}{\omega_c a}$ are 0.5.) As for the complex curves to the right of the lower branch in Figure 4.5, the equivalent curves are believed to exist to the right of the real curves on the $\omega = kV_{yo}$ axis in Figure 4.9 but were not found numerically.

The case discussed here is an intermediate one between that of sections 4.7 and 4.8. The relation to the stationary beam with velocity shear has been discussed. The relation with Figure 4.3 of section 4.7 is more complex. The "slow" curves have collapsed to the $\omega = kV_{yo}$ axis while giving rise to a

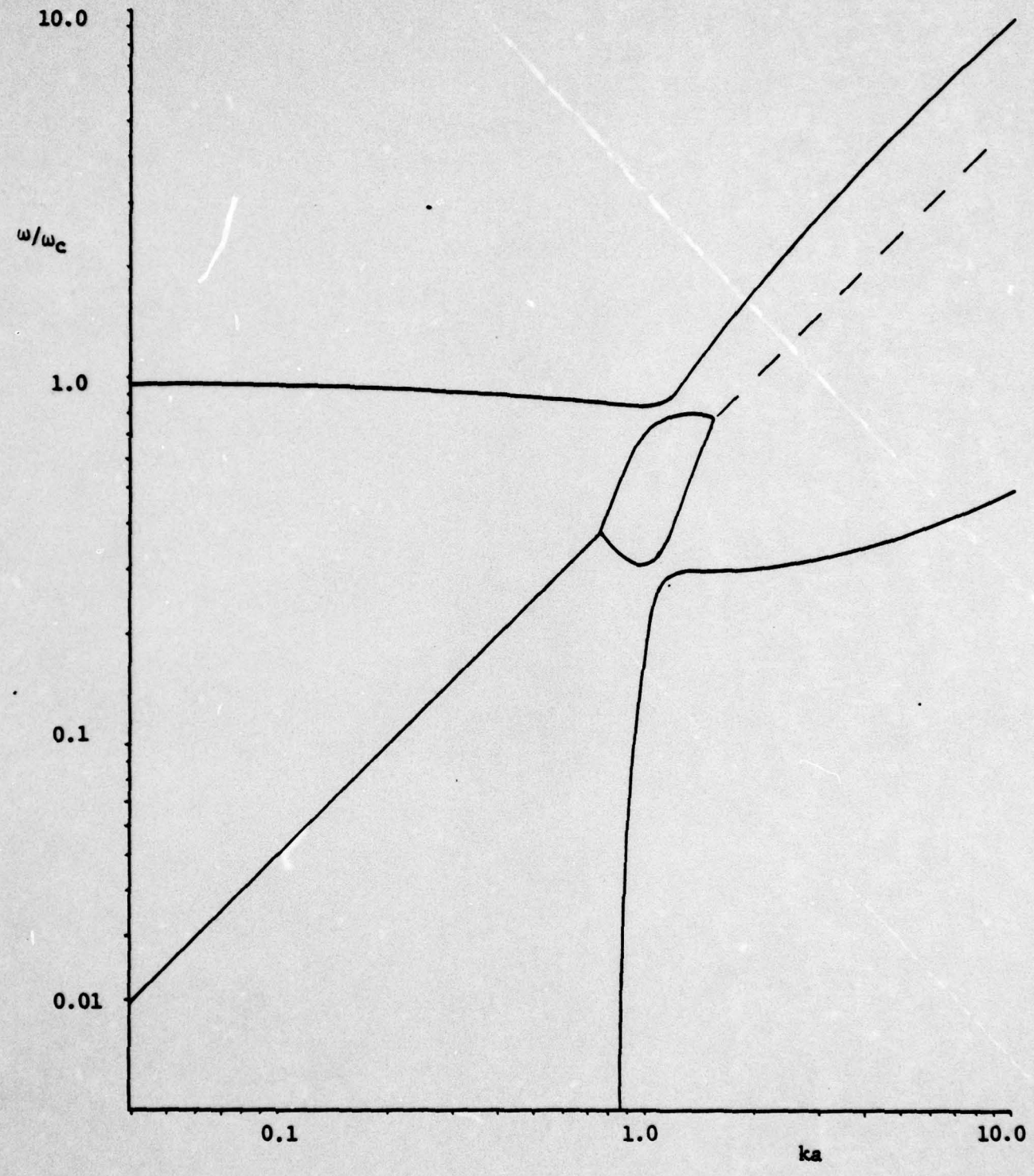

Figure 4.9

Dispersion curves for a drifting beam with velocity shear, with $\omega_p^2/\omega_c^2 = 0.5$, $V_{po}/\omega_c a = 0.5$ and $\beta = \omega_s/\omega_c = 0.5$. The curves are derived from Figure 4.5 merely by adding $\omega = kV_{yo}$ to the real part of each curve; curves are symmetrical about the line $\omega = kV_{yo}$ for a given value of k. Imaginary curves are not shown.

growing wave. Near ka = 0.7 they leave the synchronous axis to produce a symmetrical pair of dispersion curves. The "fast" curves interact the slow one, then proceed past ka = 1.5 to produce the gyroresonance curves. Their real parts likely remain close to the synchronous axis.

4.10 Application to Bending Beams

The dispersion curves presented here show the behaviour of wave modes in a straight drifting or stationary electron beam, with or without velocity shear. They represent an extension on the work of Knauer[30] and Buneman, Levy and Linson[31]. In particular, the requirement $\omega_s\omega_c = \omega_p^2$ has been eliminated in order to allow beams with arbitrary velocity shear ω_s to be analyzed. As a beam bends in crossed electric and magnetic fields, it undergoes a range of velocity shears which in turn give rise to a variety of wave modes. For example, a beam emerging from a cathode in the -x direction, and bending toward the +x direction (Figure 4.1) starts with zero velocity shear, goes through a maximum ω_s, then approaches a fixed ω_s as it enters the drift region of the tube.

The trends in dispersion curve shape which were discussed in connection with Figure 4.6 can be extrapolated with the aid of Figure 4.9 to describe the progression of wave modes as an electron beam undergoes changes. Figure 4.10 shows the changes schematically. First, as the electrons accelerate, the synchronous axis rises from a horizontal position to an angle with the k axis corresponding to the beam velocity, $\omega/k = V_{yo}$. Secondly, the velocity shear causes the two intersecting dispersion curves to go from a shallow angle to the synchronous axis, to a steep angle, and then to some constant angle. Beam acceleration will cause the value of velocity shear to be greater in regions of higher velocity, but as the beam straightens out and enters the drift region the velocity shear becomes fixed. Finally, beam convergence means that the beam width will be smaller, hence k greater for a given part of the dispersion curve. That is, the reduced beam width causes decreased wavelength.

The following picture then emerges as the beam advances from emitter to drift region. Consider a frequency ω where two surface waves exist, as marked

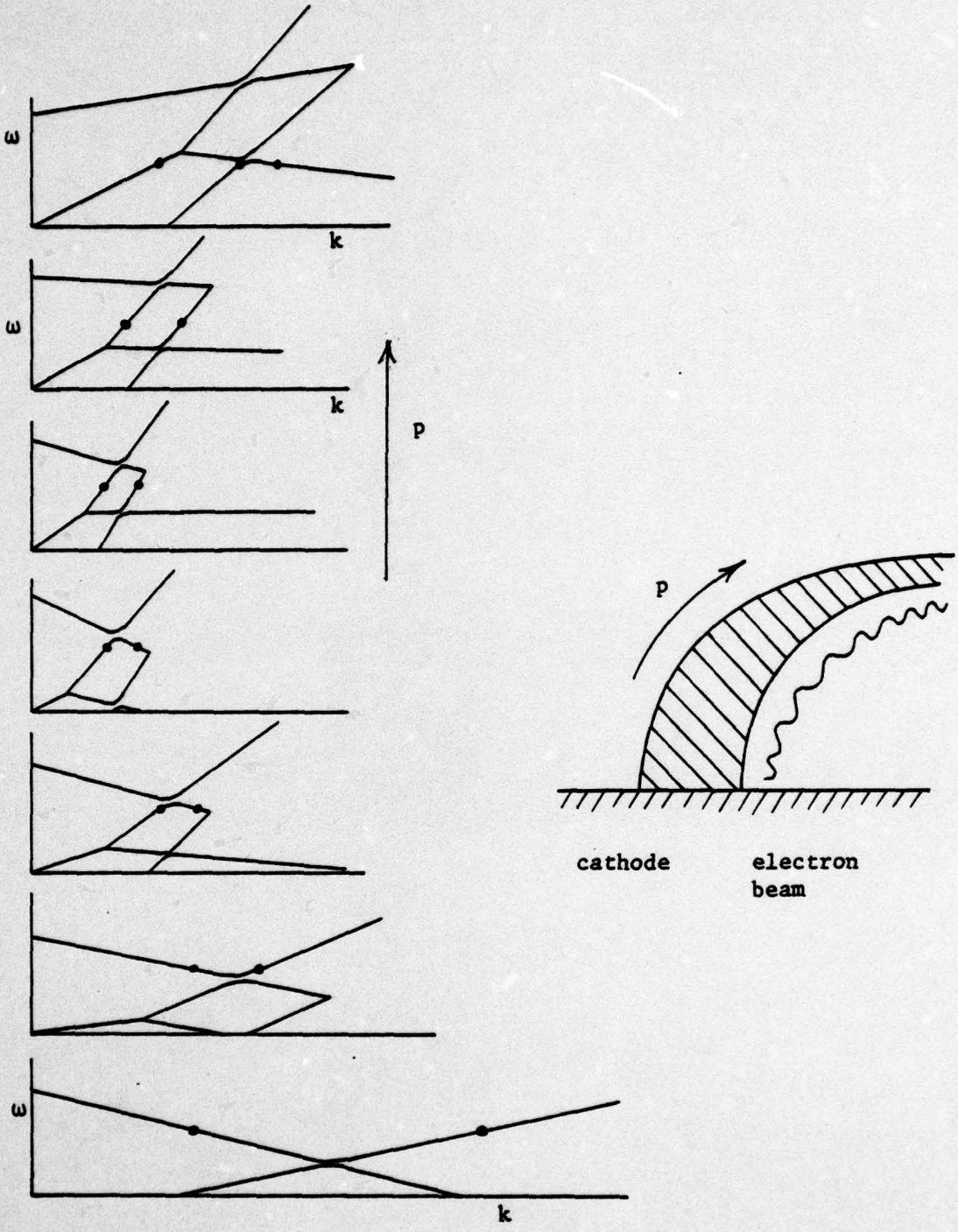

Figure 4.10

Changes in dispersion curves as beam accelerates, bends and converges in crossed electric and magnetic fields. The progression is read from the bottom up. Circles indicate the points on the curves corresponding to a fixed frequency ω. One point in the upper diagram (the left one) corresponds to a growing wave. Diagram to the right shows changes in the wavelength as perturbation travels up the beam.

on Figure 4.10. As beam velocity increases, the wavenumbers k of the two surface waves approach a common value. They then transform into a pair of bulk internal waves, at higher and lower k. As velocity continues to increase, the higher k wave begins to propagate slower than the beam velocity, while the lower k wave continues to propagate faster than beam velocity. As the beam bends into the drift region, acceleration decreases. The two bulk waves approach a common velocity at the speed of the beam, then become a growing surface wave with a large internal component. At higher frequencies bulk and surface waves also exist.

It is recognized that a plot of complex ka versus real ω/ω_c would be invaluable in determining the behaviour of wave modes at various frequencies. Such a plot was made by fixing ω and varying k. All real curves were confirmed as in the previous figures, but no solution was found with non-zero imaginary ka. Such a solution would not be expected for a stationary beam, but could be expected to exist in a drifting beam.

In extending the picture just described, dispersion curves with constant velocity shear ω_s can be a function of x, possessing first and second derivatives $\omega_s'(x)$ and $\omega_s''(x)$. Then the equation in V_x, (22) remains but equations (23) and (35) take the form

$$r = \frac{2k\omega_s(\omega - kV_{yo}) - \omega_c\omega_s'}{\Omega^2} \tag{63}$$

$$s^2 = \frac{2k\omega_s'(\omega - kV_{yo}) - \omega_c\omega_s'' - 2k^2\omega_s^2}{\Omega^2} - \left[\frac{2k\omega_s(\omega - kV_{yo}) - \omega_c\omega_s'}{\Omega^2}\right]^2$$

$$- \frac{k}{\omega - kV_{yo}}\left\{\left[k(\omega - kV_{yo}) - \omega_s'\right] + \frac{\omega_s - \omega_c}{\Omega^2}\left[2k\,\omega_s(\omega - kV_{yo}) - \omega_c\omega_s'\right]\right\}$$

$$a_\pm = k\left\{\frac{2k\,\omega_s(\omega - kV_{yo}) - \omega_c\omega_s'}{k\Omega^2} + \frac{\omega_p^2 \mp \omega_s(\omega - kV_{yo})}{(\omega - kV_{yo})\left[\omega_c \mp (\omega - kV_{yo})\right]} \pm 1\right\} \tag{64}$$

Since kinetic energy $\frac{1}{2} mV^2$ increases linearly with distance from the cathode, velocity shear is approximately quadratic across the beam. The dispersion curves have not been worked out for equations (63) and (64), but are believed to be similar in most respects to those already derived.

The dispersion curves presented in this paper have been developed using the electronic equations with several simplifications. A major simplification has been the removal of the convective terms, implying that the perturbation waves maintain a constant amplitude. If this restriction could be eliminated, a quantitative picture of the development of perturbations in bending, converging beams would be possible. Nevertheless, studies such as the present one are necessary to establish the behaviour of wave modes in drifting electron beams, and to make qualitative extensions to electron beams with varying dc conditions.

5.0 PUBLICATIONS RESULTING FROM THE AFOSR SUPPORT

The first year's effort was issued as a scientific report, MPB-112-1, entitled "Velocity Noise in a Crossed-Field Diode" and was published in Int. Journal of Electronics, Vol. 47, No. 1, pp. 17-40 (1979). Appendix I contains a copy of this article. The second year's effort is contained in Section 4 of this final report, MPB-112-2.

6.0 PERSONNEL

The principal investigator for this study program is Dr. I.P. Shkarofsky. He was assisted by Dr. I.P.W. Sinclair, an industrial post-doctoral fellow.

7.0 INTERACTIONS

Consultations on noise in crossed-beam devices were held with Prof. P.A. Lindsay on September 24, 1978, of King's College, London, U.K. Prof. Lindsay is one of the original workers in this field and has written many articles analyzing electron motion with a kinetic approach. A useful interchange of ideas arose out of this meeting.

Recently, on Sept. 24, 1979, Dr. G. Dohler of Northrop wrote us a letter expressing interest and asking for more information on our scientific report "Velocity noise in crossed-beam devices".

Dr. V. Granatstein of NRL has also discussed the above work with us and a copy was sent to him.

8.0 REFERENCES

1. Herbaugh, R.E. Some facts, some finances, some fears, and the future. Microwaves 18, No. 3, 43-52 (1979).

2. Saloom J.A. and R.A. Lee. Monterey revisited. Microwave J. 21, No. 7, 14-26, 68 (1978).

3. Skowron, J.. Oral paper at third Monterey Conference, May 1-3, 1978. (Reported by Saloom and Lee, Microwave J. 21, No. 7, 14-26,68 (1978)).

4. Maynard, E.D. Life cycle cost control of microwave transmitters. Microwave J. 20, No. 6, 70-72 (1977).

5. Osepchuk, J.M. Life begins at forty: microwave tubes. Microwave J. 21, No. 11, 51-60 (1978).

6. Osepchuk, J.M. New horizons for microwave tubes. Microwave J. 21, No. 7, 36-38 (1978).

7. IEEE Trans. ED. June 1977 Issue.

8. Shaw, E.K. and G.P. Kooyers, Computer-aided design of electron guns for injected-beam crossed-field amplifiers. IEEE ED-26, 1100 (1979).

9. Kino, G.S. A design method for crossed-field electron guns. IRE Trans ED-7, 179 (1960).

10. Masnard, N.A. and J.E. Rowe. Investigation of a convergent flow crossed-field gun. Int. J. Elect. 19, 343 (1965).

11. Lomax, R.J. Exact electrode systems for the formulation of an electron beam. J. Electron. Contr. 3, 367 (1957).

12. Kirstein, P.T. On the determination of the electrodes required to produce a given electric field distribution along a prescribed curve. Proc.Inst.Radio Engs. 46, 1716 (1958).

13. True, R. Crossed-field guns analyzed on a deformable mesh. Paper presented at Int. Elect. Services Meeting Dec. 4-6 (1978).

14. Fontana, J.P., D.M. MacGregor and J.E. Rowe. Simulation of distributed-emission and injected-beam crossed-field amplifiers. Technical Report on Contract F49620-77-C-0091. Harris SAJ, Inc. (1979).

15. Kooyers, C.P. and E.K. Shaw, Noise phenomena in crossed-field electron beams. Technical Report on Contract F49620-77-C-0061. (1979)

16. McDowell, H.L. and G.K. Farney. Crossed-field noise generation devices in Microwave Power Engineering E.C. Okress, ed. Academic Press: New York (1968).

17. Lindsay, P.A. General steady state theory of linear magnetrons. I. J. Electronics and Control 8, No. 3, 177-206 (1960).

18. Lindsay, P.A. General steady state theory of linear magnetrons II. J. Electronics and Control 17, No. 1, 67-79 (1964).

19. Ho R.Y.C. and T. Van Duzer. Approximate formulas for crossed-field, potential-minimum parameters. Trans. IEEE, ED-15, 70-74 (1968).

20. Bacal M., M. Cristescu and C. Voci. Influence of emission velocities and current density on the cut-off characteristic of a plane magnetron. Int. J. Electronics 28, No. 2, 149-171 (1970).

21. Lindsay, P.A. Velocity and potential distributions in a linear, smooth anode magnetron (magnetic diode). J. Appl. Phys. 33, 3298-3300 (1962).

22. Lindsay, P.A. and R.S. Goodwell. Velocity and potential distributions in a linear, smooth anode magnetron (magnetic diode) II. J. Appl. Phys. 36, 411-419 (1965).

23. Rack, A.J. Effect of space-charge and transit time on the shot noise in diodes. Bell System Tech. J. 17, 592-619 (1938).

24. Smullin L.D. and H.A. Haus. Noise in Electron Devices. MIT Press and Wiley & Sons, N.Y. (1959).

25. Van Duzer, T. Noise figure calculations for crossed field forward wave amplifiers. Trans. IEEE, ED-10, 370-378 (1963).

26. Bespalov, A.N. and V. Usychenko. Influence of cathode emission on the stability of oscillations in a magnetron. Sov. Phys. Tech. Phys. 21, No. 7, 881-2 (1976a).

27. Bespalov, A.N. et al. Oscillations in a magnetron diode. Sov. Phys. Tech. Phys. 21, No. 7, 882-3 (1976b).

28. MacFarlane, G.G. and H.G. Hay. Wave propagation in a slipping stream of electrons: small amplitude theory. Proc. Phys. Soc. 63, 409 (1950).

29. Gould, R.W. Space-charge effects in beam-type magnetrons. J.Appl. Phys. 28, 599 (1957).

30. Knauer, W. Diocotron instability in plasmas and gas discharges. J. Appl. Phys. 37, 602 (1966).

31. Buneman, O., R.H. Levy and L.N. Linson. Stability of crossed-field electron beams. J. Appl. Phys. 37, 3203 (1966).

32. Ho, R.Y.C. and T. Van Duzer. The effect of space-charge on shot noise in crossed-field electron guns. Trans IEEE, ED-15, 75 (1968).

33. Espinose, R.J. and R.R. Moats, Broad-band injected-beam crossed-field amplifiers. Trans IEEE, ED-24,13 (1977).

34. Cooke, M. and W. Sobotka. Noise, intermodulation and linearity in a CFA. In "MOGA 70" Kluwev-Deventer Publ., Netherlands (1970) pp. 8-25 to 8-30.

35. Abramowitz, M. and I.A. Segun. Handbook of Mathematical Functions, Dover Publications, Inc. New York: 1968.

36. Hasegawa, A. Plasma Instabilities and Non-Linear Effects. Springer-Verlag, New York: 1975.

ACKNOWLEDGEMENTS

The authors wish to acknowledge many helpful discussions with Dr. S.B. Nickerson of MPB Technologies Inc. The use of the eigenvalue technique is due to his suggestions.

We gratefully acknowledge the support from the Air Force Office of Scientific Research (AFSC), United States Air Force, under Contract No. F49620-77-C-0106.

APPENDIX I

Reprint of Article

"Velocity Noise in a Crossed-Field Planar Diode" by I.P. Shkarofsky, in International Journal of Electronics, Vol. 47, No. 1, pages 17-40, 1978.

INT. J. ELECTRONICS, 1979, VOL. 47, NO. 1, 17–40

Velocity noise in a crossed-field planar diode

I. P. SHKAROFSKY

MPB Technologies Inc., P.O. Box 160, Ste. Anne de Bellevue, Quebec, Canada, H9X 3L5.

Expressions are derived based on kinetic theory for the seven moments over the energy distribution function in a planar thermionic diode with crossed electric and magnetic fields, both for the electric-field dominated and magnetic-field dominated situations. The expressions are given as integrals over the distribution function at the cathode surface, whose form is left arbitrary. For a maxwellian form, analytic results, valid in the region of the potential minimum, are provided in the electric-field dominated limit when the potential profile is assumed to be parabolic in the vicinity of its minimum. The seven moments are the density profile, the two current flux components, the two mean velocity components and the two mean square velocity components. From the latter four moments, the velocity noise is determined. At the potential minimum, the velocity noise is minimized when $\omega_{pm}^2/\omega_c^2 = 2$ where ω_{pm} is the plasma frequency at the potential minimum and ω_c is the cyclotron frequency, and operation under this condition is recommended. It is also shown how Lindsay's, Ho and Van Duzer's and the present analyses are related to each other.

1. Introduction

The technology of crossed-field devices, if understood better, could lead to improved methods for decreasing their noise content, which is one of the main problems at high beam currents. Although many sources of noise have been postulated in the past, Ho and Van Duzer's (1968 b) theory is significant in showing that the random emission at the cathode, in conjunction with space-charge effects near the potential minimum, is a capable initial noise growth mechanism. Since their analysis tackled the problem of current shot noise, we concentrate our attention here on velocity noise. Lindsay (1960, 1964) delineates the two regimes of magnetic-field and space-charge or electric-field dominated operation of a crossed-field diode. Ho and Van Duzer's (1968 a) analysis applies to an electric-field dominated case. Here as in Lindsay (1970), we discuss its relationship to Lindsay's (1964) previous work. A controlled experiment performed by Bacal *et al.* (1970) shows the transition in the cut-off characteristic as the current is increased to an electric-field dominated condition from a magnetic-field dominated condition. When it is magnetic-field dominated at low currents, the anode current displays and abrupt cut-off as the magnetic field increases past a critical value, more or less in agreement with Lindsay's (1960) theory. At high current levels, the cut-off characteristic broadens considerably. Ho and Van Duzer's (1968 a) analysis seems to be more appropriate and the less abrupt current decrease is consistent with Bacal *et al.*'s results.

We employ a kinetic approach with an arbitrary phase-space spherically symmetric velocity distribution function at the cathode. Although numerical results

Received 20 March 1978; accepted 23 October 1978.

 0020-7217/79/4701 0017 $02.00

are calculated for a maxwellian distribution, it is just as easy to do all the calculations for other distributions using the analysis given here. Implicit in the generalization of the results to an arbitrary velocity distribution function is the necessity to work in polar coordinates, in order to reduce, after integration over angle, the phase-space integrations in three dimensions to only one over the magnitude of velocity. For this reason, we do not obtain error functions as found for a maxwellian after integration over two cartesian coordinates.

The magnetic-field dominated situation is considered briefly, followed by a more intensive analysis on the electric-field dominated case. Various moments over the distribution function are derived, such as current flow components and mean square deviations in the velocity flow. In particular, we find that the velocity noise summed over both flow components at the potential minimum, is least when $\omega_{pm}^2/\omega_c^2 = 2$ where ω_{pm} is the plasma frequency evaluated at the potential minimum and ω_c is the cyclotron frequency.

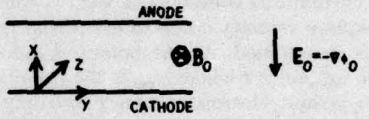

Figure 1. Geometry of a thermionic diode with crossed electric and magnetic fields.

2. General analysis

The geometry considered is shown in Fig. 1. A static electric field, $\mathbf{E}_0 = -\nabla\phi_0$, modified by space-charge effects, acts along the x-direction, and the external field, $\mathbf{B}_0$ is along the z-direction. As in Lindsay (1960), we define $\omega_c = eB_0/m$ and the normalized parameters

$$\eta = \frac{2e\phi_0}{mv_t^2}, \quad X = \frac{\omega_c x}{v_t}, \quad Y = \frac{\omega_c y}{v_t}, \quad \mathbf{w} = \frac{\mathbf{v}}{v_t} \tag{1}$$

where v_t is a convenient normalizing velocity, e.g. $v_t^2 = 2kT/m$ for a maxwellian distribution at a cathode temperature T. Also e, m, and k are respectively magnitude of electron charge, mass and Boltzmann's constant. The relations between (w_x, w_y) within the diode and their cathode values (w_{x0}, w_{y0}) are

$$\begin{gathered} w_x^2 + w_y^2 = w_{x0}^2 + w_{y0}^2 + \eta \\ w_y = w_{y0} + X \text{ and } w_x^2 = w_{x0}^2 - X(X + 2w_{y0}) + \eta \end{gathered} \tag{2}$$

This basic starting point is used in the following sections to delineate the areas in (w_{x0}, w_{y0}) space where electrons are allowed to be present and over which one integrates the various moments. In contrast to Lindsay (1960, 1964) we map the areas in the (w_{x0}, w_{y0}) plane rather than in the (w_x, w_y) plane. This is because the velocity distribution function that we use is allowed to be of an arbitrary form which is given at the cathode position. We prefer to refer all velocities back to the cathode position, rather than carrying factors such as $w_x^2 + w_y^2 - \eta$ in the argument of the velocity distribution function. As a check, all the results in the following sections were reformulated and rederived in the (w_x, w_y) variables, but this analysis is omitted here.

We use the two- and three-dimensional electron velocity distribution† function (evaluated at the cathode), denoted respectively by $f_2(w_{x0}^2, w_{y0}^2)$ and $f_3(w_{x0}^2, w_{y0}^2, w_{z0}^2)$. The basic assumption is made that these functions are spherically symmetric satisfying $f_3(w_{x0}^2, w_{y0}^2, w_{z0}^2) = f_3(w_0^2)$ and $f_2(w_{x0}^2, w_{y0}^2) = f_2(w_{\perp 0}^2)$ where $w_0^2 = w_{\perp 0}^2 + w_{z0}^2$ and $w_{\perp 0}^2 = w_{x0}^2 + w_{y0}^2$. We define f_2 in terms of f_3 as follows:

$$f_2(w_{x0}^2, w_{y0}^2) = \pi^{-1/2} \int_{-\infty}^{\infty} f_3(w_{x0}^2, w_{y0}^2, w_{z0}^2)\, dw_{z0} \tag{3}$$

The $\pi^{-1/2}$ factor is inserted for convenience so that for a maxwellian distribution, f_2 and f_3 have identical forms, namely

$$f_2(w_0^2) = f_3(w_0^2) = (2J_s/\pi v_t^4) \exp(-w_0^2) = (2n_T/\pi^{3/2} v_t^3) \exp(-w_0^2) \tag{4}$$

where

$$J_s = \int_0^{\infty} v_{x0}\, dv_{x0} \int_{-\infty}^{\infty} dv_{y0} \int_{-\infty}^{\infty} dv_{z0} f_3(v_0^2) \text{ and } n_T = \int_0^{\infty} dv_{x0} \int_{-\infty}^{\infty} dv_{y0} \int_{-\infty}^{\infty} dv_{z0} f_3(v_0^2)$$

The most general moment at position (X, Y) where the potential is η is given by

$$\begin{aligned} \bar{M}_{m,n} &= \int w_y^m\, dw_y \int w_x^n\, dw_x \int_{-\infty}^{\infty} dw_z f_3(w^2 - \eta) \\ &= \sqrt{\pi} \int (w_{y0} + X)^m\, dw_{y0} \int w_{x0}\, dw_{x0} \{[w_{x0}^2 - X(X + 2w_{y0}) + \eta]^{n-1}\}^{1/2} f_2(w_{\perp 0}^2) \end{aligned} \tag{5}$$

using eqns. (2) and (3), with no variations considered in the z-direction of the magnetic field. The square root can be positive or negative depending respectively on the sign of w_x^{n-1}. For $n = 0$, one obtains a w_{x0}/w_x factor in the integrand. This is not troublesome and no singularities appear after integration, as given later in eqn. (8). The limits on w_{x0} and w_{y0} differ for the magnetic-field and electric-field dominated cases. The following moments are derived, electron density in configuration space, n, the x- and y-directed current flux densities, J_x and J_y, the mean‡ velocities, $\bar{v}_x$ and $\bar{v}_y$ and the mean square velocities, $\overline{v_x^2}$ and $\overline{v_y^2}$. These are defined by

$$\begin{aligned} &n = v_t^3 \bar{M}_{0,0}, \qquad J_x = v_t^4 \bar{M}_{0,1}, \qquad \bar{v}_x/v_t = \bar{M}_{0,2}/\bar{M}_{0,1}, \\ &\overline{v_x^2}/v_t^2 = \bar{M}_{0,3}/\bar{M}_{0,1}, \qquad J_y = v_t^4 \bar{M}_{1,0}, \qquad \bar{v}_y/v_t = \bar{M}_{2,0}/\bar{M}_{1,0}, \\ &\overline{v_y^2}/v_t^2 = \bar{M}_{3,0}/\bar{M}_{1,0} \end{aligned} \tag{6}$$

The noise velocity components can be shown to be related to the deviations in velocity by

$$\overline{\langle v_x^2 \rangle} = 2e\Delta f[\overline{v_x^2} - (\bar{v}_x)^2]/(eA_c J_x)$$

and

$$\overline{\langle v_y^2 \rangle} = 2e\Delta f[\overline{v_y^2} - (\bar{v}_y)^2]/(eA_c J_y) \tag{7}$$

---

† Our $f_3(\mathbf{w}) = n(\mathbf{r}, \mathbf{w})/v_t^3 = f(\mathbf{w}|\mathbf{r})n(\mathbf{r})/v_t^3$ and $f_3(\mathbf{v}) = n(\mathbf{r}, \mathbf{v}) = f(\mathbf{v}|\mathbf{r})n(\mathbf{r})$ where $f(\mathbf{v}|\mathbf{r})$ and $n(\mathbf{r}, \mathbf{v})$ are commonly found in the literature, and are referred to as phase-space density functions.

‡ The means $\overline{v_{x,y}}$ and $\overline{v_{x,y}^2}$ are actually related respectively to the second- and third- order moments over $f_3(\mathbf{w})$ or $f(\mathbf{w}|\mathbf{r})$. They are the first and second moments over $f_1(\mathbf{w}|\mathbf{r})$, also found in the literature.

where Δf is the frequency bandwidth, A_e is the emitting area, and

$$\overline{\langle v_x^2\rangle} \equiv \overline{\langle(\delta\bar{v}_{xs})^2\rangle} \quad \text{and} \quad \overline{\langle v_y^2\rangle} \equiv \overline{\langle(\delta\bar{v}_{ys})^2\rangle}$$

are averaged over velocity and time. Equation (7) is based on Rack's (1938) analysis, a summary being given in Smullin and Haus (1959), and assumes that the mean square fluctuations in the velocity components are caused by shot noise. The parameters in eqn. (7) are to be evaluated at the potential minimum in the presence of space-charge.

The double integrals in eqn. (5) are transformed to a *single* integral over the $f_2(w^2)$ distribution function (omitting the $_{\perp 0}$ subscript on w^2). For this purpose,† we write $w_{x0}=w\cos\theta$ and $w_{y0}=w\sin\theta$ and integrate over θ, making sure to cover the same areas. The areas and limits are given in the following section. Here we show the results of the θ integrations, consecutively for each of the seven moments in eqn. (6), without inserting the limits. The $h_\alpha(Z)$ functions result after integration over θ or $Z\equiv\sin\theta$, with $\alpha=0,1\ldots,6$, where

$$h_\alpha(Z(w))=\int^{Z(w)}(X+wZ)^m[w^2+\eta-(X+wZ)^2]^{(n-1)/2}\,dZ$$

After inserting the limits, Z becomes a function of w. We obtain

$$\bar{M}_{m,n}=\sqrt{\pi}\int w f_2(w^2)h_\alpha(Z(w))\,dw$$

with

$$\begin{aligned}
&h_0(Z)=\sin^{-1}u, \quad u\equiv(wZ+X)/(w^2+\eta)^{1/2}\\
&h_1(Z)=wZ, \quad h_2(Z)=\tfrac{1}{2}(\eta+w^2)[\sin^{-1}u+u(1-u^2)^{1/2}]\\
&h_3(Z)=(wZ+X)[\eta+w^2-\tfrac{1}{3}(wZ+X)^2]-X(w^2+\eta-\tfrac{1}{3}X^2)\\
&\qquad\equiv h_3'(Z)-X(w^2+\eta-\tfrac{1}{3}X^2) \qquad (8)\\
&h_4(Z)=-[w^2+\eta-(wZ+X)^2]^{1/2}\\
&h_5(Z)=\tfrac{1}{2}(\eta+w^2)[\sin^{-1}u-u(1-u^2)^{1/2}]\\
&h_6(Z)=[w^2+\eta-(wZ+X)^2]^{1/2}\{\tfrac{1}{3}[w^2+\eta-(wZ+X)^2]-w^2-\eta\}
\end{aligned}$$

In $h_3(Z)$, we use $h_3'(Z)$ to designate the Z-dependent part since the other part cancels after inserting the upper and lower limits.

The subscripts, 0, 1, ..., 6 refer respectively to the moments n, J_x, $\bar{v}_x$, $\overline{v_x^2}$, J_y, $\bar{v}_y$ and $\overline{v_y^2}$. In the following sections, the limits on w and on θ, the latter giving $Z(w)$, are provided.

† For simplicity in notation, we use as the dummy variable of integration w instead of $w_{\perp 0}$ to designate $(w_{x0}^2+w_{y0}^2)^{1/2}$ at the cathode. It should not be confused with its other use to designate the normalized velocity within the diode.

3. Magnetic-field dominated results

This case is defined by the condition that $\gamma > \gamma_a$ throughout the diode, where

$$\gamma \equiv \tfrac{1}{2}\left(\frac{\eta}{X} - X\right)$$

and

$$\gamma_a \equiv \tfrac{1}{2}\left(\frac{\eta_a}{X_a} - X_a\right) \tag{9}$$

Subscript 'a' refers to values at the anode. Figure 6 in Lindsay (1960) shows shaded areas of accessibility of electrons in a w_y versus w_x plot based on eqn. (2). We prefer to work in the (w_{x0}, w_{y0}) plane and the equivalent plot† is shown here in Fig. 2, with

$$w_{x0A}^2 \equiv -\eta_a + X_a^2 + 2X_a w_{y0} \quad \text{and} \quad w_{x0B}^2 \equiv -\eta + X^2 + 2X w_{y0} \tag{10}$$

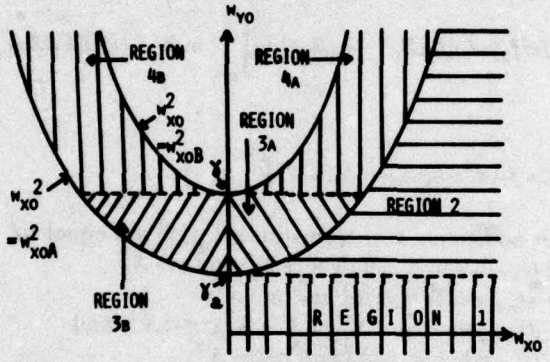

Figure 2. Electron velocity regions of accessibility, shown shaded, on a w_{y0} versus w_{x0} plot, when $\gamma > \gamma_a$, the magnetic-field dominated case.

These represent the w_{x0} values that allow electrons to reach the anode at X_a or point X respectively. For the moments, J_x and $\overline{v_x^2}$, n is odd and the contributions from regions 3.4 and $4A$ cancel those from regions $3B$ and $4B$. Thus the limits on the integrals in eqn. (5) are given by

$$\int dw_{y0} \cdots \int dw_{x0} \cdots = \int_{-\infty}^{\gamma_a} dw_{y0} \cdots \int_0^{\infty} dw_{x0} \cdots + \int_{\gamma_a}^{\infty} dw_{y0} \cdots \int_{w_{x0A}}^{\infty} dw_{x0} \cdots \tag{11}$$

For the other moments, $n, J_y, \bar{v}_x, \bar{v}_y$, and $\overline{v_y^2}$, the whole area has to be included. Rather than cancelling, the above indicated contributions add, giving

$$\int dw_{y0} \cdots \int dw_{x0} \cdots = \int_{-\infty}^{\gamma_a} dw_{y0} \cdots \int_0^{\infty} dw_{x0} \cdots + \int_{\gamma_a}^{\infty} dw_{y0} \cdots \int_{w_{x0A}}^{\infty} dw_{x0}$$
$$+ 2\int_{\gamma_a}^{\gamma} dw_{y0} \cdots \int_0^{w_{x0A}} dw_{x0} \cdots + 2\int_{\gamma}^{\infty} dw_{y0} \cdots \int_{w_{x0B}}^{w_{x0A}} dw_{x0} \cdots \tag{12}$$

† Region 1 in our Fig. 2 corresponds to the shaded area below $w_y = w_{y4}$ in Lindsay (1960), region 2 to that between $w_y = w_{yA}$ and $w_y = w_{y4}$, region $3A$ to that bounded by $w_y = w_{y2}$, w_{yA} and w_{yB} on the right-hand side and region $3B$ to the same on the left-hand side, region $4A$ to that bounded by the $w_x = 0$ axis, $w_y = w_{y2}$ and w_{yA} on the right-hand side and region $4B$ to the same on the left-hand side. Areas to the left, which image those on the right, correspond to particles turning around and arriving back at the cathode.

As outlined above in eqn. (8), we change to polar coordinates and cover the same areas in integration over w and θ with $w_{x0}=w\cos\theta$ and $w_{y0}=w\sin\theta$. The following $Z(w)$ functions occur:

$$Z_{0,1}=\pm 1,\ Z_{2,3}(w)=[-X\pm(w+\eta)^{1/2}]/w$$

and

$$Z_6(w)=[-X_a+(w^2+\eta_a)^{1/2}]/w \tag{13}$$

and the following positive definite limits on w are needed:

$$w_{0a}^2=-\eta \quad \text{when} \quad \eta<0, \quad w_{0h}^2=\tfrac{1}{4}\left(\frac{\eta_a}{X_a}-X_a\right)^2 \quad \text{and} \quad w_{0i}^2=\tfrac{1}{4}\left(\frac{\eta}{X}-X\right)^2 \tag{14}$$

The detailed algebra is omitted. We find that eqn. (11) is equal to $G_{\alpha,D}$ or $G_{\alpha,E}$ when $\gamma_a>0$ or $\gamma_a<0$ respectively, where

$$G_{\alpha,D}=\int_0^{w_{0h}} w\,dw f_2(w^2)[h_\alpha(Z_0)-h_\alpha(Z_1)]+\int_{w_{0h}}^{\infty} w\,dw f_2(w^2)[h_1(Z_6)-h_1(Z_1)] \tag{15}$$

and

$$G_{\alpha,E}=\int_{w_{0h}}^{\infty} w\,dw f_2(w^2)[h_\alpha(Z_6)-h_\alpha(Z_1)] \tag{16}$$

Also the latter additional two terms in eqn. (12) are equal to

(i) $G_{\alpha,F}-G_{\alpha,D}$ when $\gamma_a>0$ or $\eta_a>X_a^2$ and $\eta>X^2$.
(ii) $G_{\alpha,G}-G_{\alpha,E}$ when $\eta_a<X_a^2$ and $\eta>X^2$.
(iii) $G_{\alpha,H}-G_{\alpha,E}$ when $\eta_a<X_a^2$ and $-X^2<\eta<X^2$, and
(iv) $G_{\alpha,I}-G_{\alpha,E}$ when $\eta_a<X_a^2$ and $\eta<-X^2$.

The additional G functions are given by

$$\begin{aligned}G_{\alpha,F}=&2\int_0^{w_{0i}} w\,dw f_2(w^2)[h_\alpha(Z_0)-h_\alpha(Z_2)]\\&+\int_{w_{0h}}^{\infty} w\,dw f_2(w^2)[2h_\alpha(Z_2)-h_\alpha(Z_6)-h_\alpha(Z_1)]\\&+\int_0^{w_{0h}} w\,dw f_2(w^2)[2h_\alpha(Z_2)-h_\alpha(Z_1)-h_\alpha(Z_0)]\end{aligned} \tag{17}$$

$$\begin{aligned}G_{\alpha,G}=&2\int_0^{w_{0i}} w\,dw f_2(w^2)[h_\alpha(Z_0)-h_\alpha(Z_2)]\\&+2\int_0^{\infty} w\,dw f_2(w^2)[h_\alpha(Z_2)-h_\alpha(Z_1)]\\&+\int_{w_{0h}}^{\infty} w\,dw f_2(w^2)[h_\alpha(Z_1)-h_\alpha(Z_6)]\end{aligned} \tag{18}$$

$$\begin{aligned}G_{\alpha,H}=&2\int_{w_{0i}}^{\infty} w\,dw f_2(w^2)[h_\alpha(Z_2)-h_\alpha(Z_1)]\\&+\int_{w_{0h}}^{\infty} w\,dw f_2(w^2)[h_\alpha(Z_1)-h_\alpha(Z_6)]\end{aligned} \tag{19}$$

and

$$G_{\alpha,I}=2\int_{w_{0c}}^{\infty} w\,dw f_2(w^2)[h_\alpha(Z_2)-h_\alpha(Z_3)]$$
$$+2\int_{w_{0i}}^{\infty} w\,dw f_2(w^2)[h_\alpha(Z_3)-h_\alpha(Z_1)]$$
$$+\int_{w_{0h}}^{\infty} w\,dw f_2(w^2)[h_\alpha(Z_1)-h_\alpha(Z_6)] \tag{20}$$

In terms of the G functions, the moments are determined by

$$\left.\begin{aligned} &n=v_t^3\sqrt{\pi}G_{0,D/E/G/H/I}, \quad J_x=v_t^4\sqrt{\pi}G_{1,D/E}, \quad \bar{v}_x=(v_t^5\sqrt{\pi/J_x})G_{2,F/G/H/I},\\ &\overline{v_x^2}=(v_t^6\sqrt{\pi/J_x})G_{3,D/E}, \quad J_y=v_t^4\sqrt{\pi}G_{4,F/G/H/I}, \quad \bar{v}_y=(v_t^5\sqrt{\pi/J_y})G_{5,F/G/H/I},\\ &\overline{v_y^2}=(v_t^6\sqrt{\pi/J_y})G_{6,F/G/H/I} \end{aligned}\right\} \tag{21}$$

where D/E or $F/G/H/I$ signifies the use of one of these subscripts in the appropriate case, and the h_α functions with $\alpha=0\ldots.6$ are given in eqn. (8).

The integrals usually require numerical integration for given $f_2(w^2)$ functions such as a maxwellian. However, for J_x and the maxwellian distribution in eqn. (4), the following analytical result is obtained, being the same both for $G_{1,D}$ and $G_{1,E}$.

$$J_x=\frac{J_s}{2}\left\{1+\Phi\left(\frac{\eta_a}{2X_a}-\frac{X_a}{2}\right)+\exp(\eta_a)\left[1-\Phi\left(\frac{\eta_a}{2X_a}+\frac{X_a}{2}\right)\right]\right\} \tag{22}$$

where Φ is an error function. This is identical to Lindsay's (1960) formula and it involves only anode parameters. As shown by Bacal *et al.* (1970), J_x decreases with B_0 abruptly above a critical magnetic field given by $(X_a-\eta_a/X_a)>2$.

4. Electric-field dominated results

The electric-field dominated case is characterized by $\gamma_a>\gamma$ (see eqn. (9)). Lindsay (1964) considers this case, but he does not make much headway since his integrals cannot be formulated properly before the space-charge distribution is known. Ho and Van Duzer (1968 a), assume a parabolic spatial variation in potential and derive an expression for J_x based on certain approximations. Below we make use of the parabolic potential variation in the vicinity of the potential minimum. With the same assumption, Lindsay (1970) provides results for n, J_x and J_y. Here, we obtain results for all the seven moments based on an arbitrary velocity distribution function at the cathode. In the following section, we clarify the relationships between the above papers.

Consider eqn. (2). Since $w_x^2\geqslant 0$, we require $w_{y0}\leqslant(w_{y0})_{max}=\frac{1}{2}[\eta/X-X+(w_{x0}^2)/X]_{min}$. The maximum value of w_{y0} occurs at some position X_1 which depends on w_{x0} and $\eta(X)$. To find this, equate $\partial w_{y0}/\partial X_1=0$ to yield

$$(w_{x0}^2)_{min}=-X_1^2+X_1\eta'(X_1)-\eta(X_1)$$

and (23)

$$(w_{y0})_{max}=\tfrac{1}{2}\eta'(X_1)-X_1, \eta'\equiv\partial\eta(X)/\partial X$$

valid for $0<X<X_a$. (For a magnetic-field dominated case, X_1 does not exist.) Unfortunately one cannot solve to eliminate X_1 between $(w_{y0})_{max}\equiv w_{y0C}$ and $(w_{x0})_{min}\equiv w_{x0C}$ before $\eta(X)$ is known. The w_{x0C} curve is the relationship between the $(w_{x0})_{min}$ and $(w_{y0})_{max}$ velocities required for electrons to turn around at point X_1.

Define w_{x0A}^2 and w_{x0B}^2 as in eqn. (10) and also

$$w_{x0C}^2 = X_1(X_1 + 2w_{y0}) - \eta(X_1) \tag{24}$$

At $X = X_1(w_{y0})$, we obtain by differentiating w_{x0C}

$$\left(\frac{\partial w_{x0}}{\partial w_{y0}}\right)_{X=X_1} = \frac{X_1}{w_{x0}(X_1)} + \left\{\frac{1}{2w_{x0}}\frac{\partial X_1}{\partial w_{y0}}[2X_1 + 2w_{y0} - \eta'(X_1)]\right\}_{X=X_1} = \frac{X_1}{w_{x0}(X_1)} \tag{25}$$

in view of eqn. (23). Differentiation of eqn. (10) for w_{x0B} and w_{x0A} gives the same result at points $X_1 = X$ and $X_1 = X_a$ respectively. Since the slopes are the same, we have at least proven that the w_{w0C} curve (i.e. the $(w_{y0})_{max}$ versus $(w_{x0})_{min}$ plot) is tangent to the w_{x0A} and w_{x0B} parabolas for any $\eta(X)$ variations. As shown by Lindsay (1970), this is also true in a (w_x, w_y) plane, namely that the w_{xC} curve is tangent to both the w_{xA} and w_{xB} curves at their meeting points. Referring to Fig. 4 in Lindsay (1964), this points towards the situation in his Fig. 4 (*a*), with w_{yC} touching, rather than cutting, the w_{yA} and w_{yB} curves. Also for a parabolic $\eta(X)$ variation, the w_{yC} curve reduces to a straight line.

As before, we prefer to work in the (w_{x0}, w_{y0}) plane rather than the (w_x, w_y) plane. The equivalent of Fig. 4 (*a*) in Lindsay (1964) is shown here† in Fig. 3. Point 3 is where the w_{x0C} curve, drawn here as a straight line, touches the w_{x0B} curve. Points 7 and 5 on the negative side are where it touches the w_{x0A} curve. For conditions in the vicinity of the potential minimum where $X = X_m$, the important integration regions over velocity occur around point 3. A straight line portion is assumed here for the w_{x0C} curve, which as we show below is exact for a parabolic $\eta(X)$ variation.

Since from eqns. (10) and (24), point 3 satisfies the condition $X = X_1$, the slope of the straight line, using eqns. (23) and (25), is given by

$$\frac{\partial w_{y0}}{\partial w_{x0}} = \frac{w_{x0}(X)}{X} = \left[\frac{\eta'}{X} - \frac{\eta}{X^2} - 1\right]^{1/2}$$

The coordinates of point 3 are given in eqn. (23), namely $w_{x0} = (X\eta' - \eta - X^2)^{1/2}$ and $w_{y0} = \frac{1}{2}\eta' - X$. Consequently, the straight line through point 3 with the above slope has the equation

$$w_{y0} = \pm w_{x0}\left[\frac{\eta'}{X} - \frac{\eta}{X^2} - 1\right]^{1/2} + \frac{\eta}{X} - \frac{\eta'}{2} \tag{26}$$

The plus sign applies to positive w_{x0} and the negative sign to negative w_{x0} values. Define

$$\alpha \equiv -2\eta(X)/X + \eta'(X) \quad \text{and} \quad \beta \equiv [X\eta'(X) - \eta(X)]/X^2 \tag{27}$$

---

† In Fig. 4 (*a*) in Lindsay (1964), draw an image curve of w_{yC} on the right extending from $w_y = w_{y6}$ to $w_y = w_{y5}$. Region 1 in our Fig. 3 corresponds to the shaded region below $w_y = w_{y4}$ in Lindsay, region $2A$ to that between $w_y = w_{y6}$ and $w_y = w_{y4}$, region $2B$ to that to the right of the w_{yC} image curve between $w_y = w_{y6}$ and $w_y = w_{y5}$, region 3 to that above $w_y = w_{y5}$ and to the right of the w_{yA} curve, region $4A$ to that bounded by the $w_x = 0$ axis, the w_{yC} image curve and $w_y = w_{y1}$ on the right-hand side and region $4C$ to its image on the left-hand side, region $4B$ to that bounded by the $w_x = 0$ axis, $w_y = w_{y1}$, $w_y = w_{y5}$ and the w_{yC} image curve on the right-hand side and region $4D$ to its image on the left-hand side, region $5A$ to that bounded by the $w_x = 0$ axis, $w_y = w_{y5}$ and the curve w_{yA} on the right-hand side and region $5B$ to the same on the left-hand side. Similar remarks apply to the (w_x, w_y) plot, Fig. 4, in Lindsay (1970).

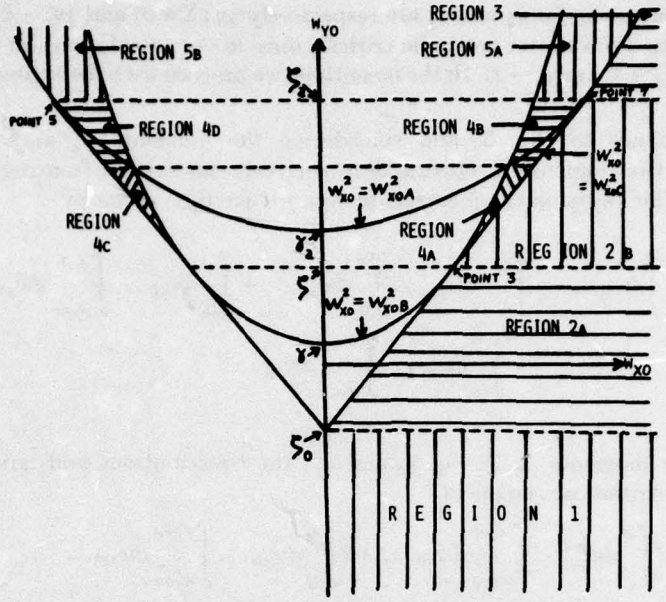

Figure 3. Electron velocity regions of accessibility, shown shaded, on a w_{y0} versus w_{x0} plot, when $\gamma_a > \gamma$, the electric-field dominated case.

and at the potential minimum where $\eta' = 0$: $\alpha = -2\eta_{r_1}/X_m$ and $\beta = -\eta_m/X_m^2$. This results in

$$\eta(X) = -\alpha X + \beta X^2 \quad \text{and} \quad \eta'(X) = -\alpha + 2\beta X \tag{28}$$

which is the form of a parabolic potential variation. We assume α and β to be constants or slowly varying functions of X. Then we can deduce the relation for X_1 from eqn. (23) and write eqn. (26) for the w_{x0C} line as

$$X_1 = \pm(2w_{y0} + \alpha)/[2(\beta - 1)] = \pm w_{x0}/(\beta - 1)^{1/2}$$

and

$$w_{y0} = -\frac{\alpha}{2} \pm (\beta - 1)^{1/2} w_{x0} \quad \text{or} \quad w_{x0} = \pm(2w_{y0} + \alpha)/[2(\beta - 1)^{1/2}] \tag{29}$$

This is a somewhat roundabout way of obtaining eqn. (29), but the method serves to justify and somewhat generalize the assumption of a parabolic potential variation. From eqns. (9) and (28), the electric-field dominated case, $\gamma_a > \gamma$, requires

$$\beta > 1 \tag{30}$$

With eqn. (29), several w_{y0} ordinate values shown in Fig. 3 can be obtained. Using eqns. (10) and (29), we note that $w_{x0C} = 0$ for point ζ_0 and $w_{x0C} = w_{x0A}$ for ζ_a, giving

$$\left.\begin{aligned} \zeta_0 &= -\alpha/2,\ \zeta = \tfrac{1}{2}\eta' - X = -\frac{\alpha}{2} + (\beta - 1)X \\ \zeta_a &= -\frac{\alpha}{2} + (\beta - 1)X_a \end{aligned}\right\} \tag{31}$$

The exact expressions for ζ_0 and ζ_a are respectively $\frac{1}{2}\eta'(X=0)$ and $\frac{1}{2}\eta'_a - X_a$. Their exact values are shown later not to be critical, since in our calculations, in fact, we later assume $\zeta_0 \to \infty$ and $\zeta_a \to \infty$. In the meantime, we proceed with the expressions in eqn. (31).

With reference to Fig. 3, and considering the moments J_x and $\overline{v_x^2}$, the contributions from regions $4A$, $4B$ and $5A$ respectively cancel those from regions $4C$, $4D$ and $5B$. The limits on the integrals in eqn. (5) are then given by

$$\int dw_{y0} \cdots \int dw_{x0} \cdots = \int_{-\infty}^{\zeta_0} dw_{y0} \cdots \int_0^{\infty} dw_{x0} \cdots + \int_{\zeta_0}^{\zeta_a} dw_{y0} \cdots \int_{w_{x0C}}^{\infty} dw_{x0} \cdots + \int_{\zeta_a}^{\infty} dw_{y0} \cdots \int_{w_{x0A}}^{\infty} dw_{x0} \cdots \tag{32}$$

For the other moments, n, J_y, $\bar{v}_x$, $\bar{v}_y$ and $\overline{v_y^2}$, the contributions add, giving the additional contributions, equal to

$$2\int_{\zeta}^{\zeta_a} dw_{y0} \cdots \int_{w_{x0B}}^{w_{x0C}} dw_{x0} \cdots + 2\int_{\zeta_a}^{\infty} dw_{y0} \cdots \int_{w_{x0B}}^{w_{x0A}} dw_{x0} \cdots \tag{33}$$

In eqn. (8), we change from cartesian to polar coordinates, covering the same areas with $w_{x0} = w\cos\theta$ and $w_{y0} = w\sin\theta$. The following $Z(w)$ functions occur in addition to those in eqn. (13):

$$\left.\begin{aligned} Z_{4,5}(w) &= \frac{1}{w}\left[-\frac{\alpha}{2\beta} \pm \left(\frac{\beta-1}{\beta}\right)^{1/2}\left(w^2 - \frac{\alpha}{4\beta}\right)^{1/2}\right] \\ Z_7(w) &= -\alpha/2w \\ Z_8(w) &= \left[-\frac{\alpha}{2} + (\beta-1)X_a\right]\Big/ w \end{aligned}\right\} \tag{34}$$

The following positive definite limits on w occur:

$$\left.\begin{aligned} w_{0a}^2 &= -\eta = \alpha X - \beta X^2 \text{ when } \eta > 0 \\ w_{0b}^2 &= \alpha^2/4\beta \\ w_{0c}^2 &= \alpha^2/4 \\ w_{0d}^2 &= \alpha^2/4 - \alpha X(\beta-1) + \beta(\beta-1)X^2 \\ w_{0e}^2 &= \alpha^2/4 - \alpha X_a(\beta-1) + \beta(\beta-1)X_a^2 \end{aligned}\right\} \tag{35}$$

Integration in polar coordinates of eqns. (5), (32) and (33) yields, after lengthy algebra, the following result with the $h_a(Z)$ functions in eqn. (8) for the sum of the three contributions in eqn. (32), which we denote by $G_{a,A}$.

$$G_{a,A} = \int_{w_{0b}}^{\infty} w\,dw f_2(w^2)\,[h_a(Z_4) - h_a(Z_5)] + \int_{w_{0c}}^{\infty} w\,dw f_2(w^2)[h_a(Z_5) - h_a(Z_1)] + \int_{w_{0e}}^{\infty} w\,dw f_2(w^2)[h_a(Z_6) - h_a(Z_4)] \tag{36}$$

The additional contributions in eqn. (33) depend on whether $X \gtrless X_m$, where $X_m = \alpha/2\beta$ is given by eqn. (28) with $\eta_m' = 0$ at the potential minimum. We find that these terms are equal to $G_{\alpha,B} - G_{\alpha,A}$ if $X > X_m$ and $G_{\alpha,C} - G_{\alpha,A}$ if $X < X_m$, where

$$G_{\alpha,B} = \int_{w_{0b}}^{\infty} w\,dw f_2(w^2)[h_\alpha(Z_4) - h_\alpha(Z_5)] + 2\int_{w_{0d}}^{\infty} w\,dw f_2(w^2)[h_\alpha(Z_2) - h_\alpha(Z_4)]$$
$$+ \int_{w_{0c}}^{\infty} w\,dw f_2(w^2)[h_\alpha(Z_5) - h_\alpha(Z_1)] + \int_{w_{0e}}^{\infty} w\,dw f_2(w^2)[h_\alpha(Z_4) - h_\alpha(Z_6)] \quad (37)$$

and

$$G_{\alpha,C} = 2\int_{w_{0a}}^{\infty} w\,dw f_2(w^2)[h_\alpha(Z_2) - h_\alpha(Z_3)] + \int_{w_{0b}}^{\infty} w\,dw f_2(w^2)[h_\alpha(Z_5) - h_\alpha(Z_4)]$$
$$+ 2\int_{w_{0d}}^{\infty} w\,dw f_2(w^2)[h_\alpha(Z_3) - h_\alpha(Z_5)] + \int_{w_{0c}}^{\infty} w\,dw f_2(w^2)[h_\alpha(Z_5) - h_\alpha(Z_1)]$$
$$+ \int_{w_{0e}}^{\infty} w\,dw f_2(w^2)[h_\alpha(Z_4) - h_\alpha(Z_6)] \quad (38)$$

In terms of the G functions, the moments are determined by

$$n = v_t^3\sqrt{\pi}G_{0,B/C}, \qquad J_x = v_t^4\sqrt{\pi}G_{1,A}, \qquad \bar{v}_x = (v_t^5\sqrt{\pi}/J_x)G_{2,B/C},$$
$$\overline{v_x^2} = (v_t^6\sqrt{\pi}/J_x)G_{3,A}, \qquad J_y = v_t^4\sqrt{\pi}G_{4,B/C}, \qquad \bar{v}_y = (v_t^5\sqrt{\pi}/J_y)G_{5,B/C},$$
$$\overline{v_y^2} = (v_t^6\sqrt{\pi}/J_y)G_{6,B/C} \quad (39)$$

where B/C signifies the use of subscript B if $X > X_m$ and C if $X < X_m$.

5. Relationship of our J_x equation to those of Lindsay, and Ho and Van Duzer

For a maxwellian distribution, the relation for J_x, obtained from eqns. (4), (8), (13), (34), (35), (36) and (39), reduces to

$$J_x = \frac{J_s}{2}\left\{1 - \Phi\left(\frac{\alpha}{2}\right) + \left(\frac{\beta-1}{\beta}\right)^{1/2}\exp\left(-\frac{\alpha^2}{4\beta}\right)\left[\Phi\left(\frac{\alpha}{2}\left(\frac{\beta-1}{\beta}\right)^{1/2}\right)\right.\right.$$
$$\left. + \Phi\left(\left(\beta X_a - \frac{\alpha}{2}\right)\left(\frac{\beta-1}{\beta}\right)^{1/2}\right)\right]$$
$$\left. + \exp(\eta_a)\left[1 - \Phi\left(\beta X_a - \frac{\alpha}{2}\right)\right]\right\} \quad (40)$$

where Φ is the error function. This equation is independent of X. We obtain the same result from Lindsay's (1964) eqn. (7.4), where $\pi^{-1/2}$ in front of the integral on the last line should read $2\pi^{-1/2}$ and vice versa on the previous line, namely

$$J_x = \frac{J_s}{2}\left\{1 + \Phi\left(\frac{\eta_c'}{2}\right) + \frac{2}{\sqrt{\pi}}\int_{\eta_c'^{/2}}^{1/2\eta_a' - X_a} \exp[-(w_{y0} + X_1)^2 + \eta_1]\,dw_{y0}\right.$$
$$\left. + \exp(\eta_a)[1 - \Phi(\eta_a'/2)]\right\} \quad (41)$$

if we can insert the parabolic form for η from equation (28), X_1 from eqn. (29) and let $\eta_c' = \eta'(X=0)$. Equation (40) is also given in Lindsay (1970) upon noting that his parameter a is $(\beta-1)^{1/2}$, but one has to omit the $\frac{1}{2}$ typographical error in front of the middle term in his eqn. (4.13). Our equation assumes a parabolic potential but allows arbitrary velocity distribution functions, whereas Lindsay's formula either does not specify the potential variation (1960) or adopts a parabolic variation (1970) but always specifies a maxwellian distribution function. If $\eta(X)$ is not given, $X_1(w_{y0})$ is unknown and the integral in eqn. (41) cannot be manipulated. Under both assumptions of a parabolic potential and a maxwellian distribution, eqns. (40) and (41) agree. Ho and Van Duzer (1968 a) use both assumptions and in addition they address the limit when the anode is far away ($X \to \infty$) and need not be considered in the region of the potential minimum. In this limit and provided β is somewhat greater than one, the two Φ terms in eqn. (40) containing X_a approach one, yielding

$$J_x = \frac{J_s}{2}\left\{1 - \Phi\left(\frac{\alpha}{2}\right) + \left(\frac{\beta-1}{\beta}\right)^{1/2} \exp\left(-\frac{\alpha^2}{4\beta}\right)\left[1 + \Phi\left(\frac{\alpha}{2}\left(\frac{\beta-1}{\beta}\right)^{1/2}\right)\right]\right\} \tag{42}$$

This is identical to Ho and Van Duzer's result who use the notation $\Omega = \omega_c(\beta-1)^{1/2}$, $\eta_m = -\alpha^2/4\beta$, and $2\omega_c x_m (m/2kT)^{1/2} = \alpha/\beta$. Thus our result is the same as Ho and Van Duzer's in the limit of $X_a \to \infty$ and with a maxwellian distribution. Finally, Lindsay's result reduces to Ho and Van Duzer's in the limits of $X_a \to \infty$ and a parabolic spatial potential.

Ho and Van Duzer (1968 a) proceed to apply a further simplification, namely that the potential minimum is deep and close to the cathode, i.e. $x_m \to 0$. This essentially means that $\alpha^2/4 > 1$ and $\beta > 1$ but $\alpha^2/4\beta$ can be of order one, since from eqns. (1) and (27):

$$\alpha = -2\eta_m/X_m = -4e\phi_m/(m x_m \omega_c v_0) \quad \text{and} \quad \beta = -\eta_m/X_m^2 = -2e\phi_m/(m x_m^2 \omega_c^2) \tag{43}$$

Equation (42) reduces to the following, which Ho and Van Duzer show to be a good approximation:

$$J_x = J_s\left(\frac{\beta-1}{\beta}\right)^{1/2} \exp\left(-\frac{\alpha^2}{4\beta}\right) = J_s \exp(\eta_m) \Big/ \left(1 + \frac{\omega_c^2}{\Omega^2}\right)^{1/2} \tag{44}$$

Generally we require that $\beta \geqslant 1{\cdot}5$ and $\alpha \geqslant 3{\cdot}2$ for the error functions to approach one. This decrease of J_x with magnetic field for an electric-field dominated case is much slower than for the magnetic field dominated case, as is indeed observed by Bacal *et al.* (1970).

6. Simplifications when $\beta \geqslant 1{\cdot}5$, $\alpha \geqslant 3{\cdot}2$ and $X_a \gg 1$ for the electric-field dominated case and calculated results

We simplify our relations in eqn. (39) in the limits of small x_m and large x_a, adopted by Ho and Van Duzer (1968 a), equivalent to $\beta \geqslant 1{\cdot}5$, $\alpha \geqslant 3{\cdot}2$ and $X_a \gg 1$. In

eqn. (35), we retain w_{0a}, w_{0b} and w_{0d} (which is equal to w_{0b} at $X = X_m$), but we let $w_{0c} \to \infty$ and $w_{0e} \to \infty$ (equivalent to $\zeta_0 \to -\infty$ and $\zeta_a \to \infty$). Thus $G_{a,A}$ reduces to the first term in eqn. (36), $G_{a,B}$ to the first two terms in eqn. (37) and $G_{a,C}$ to the first three terms in eqn. (38).

These expressions can be further drastically reduced. (See the Appendix.)

Define the function:

$$p_a(t,a) = \int_0^\infty dw\, w f_3(w^2 - a)(w^2 + t - a)^{a/2} \tag{45}$$

All the moments in eqn. (39) can be written in terms of p_a after inserting the equations in the Appendix and noting that $w_{0b}^2 = -\eta_m$. The following expressions are obtained:

$$\left.\begin{aligned}
&n(X > X_m) = -n(X < X_m) + 4\pi v_t^3 p_1(\eta,\eta) = 2\pi v_t^3 [p_1(\eta,\eta_m) - (\eta - \eta_m)^{1/2} p_0(0,\eta_m)] \\
&J_x = \pi v_t^4 [(\beta-1)/\beta]^{1/2} p_2(\eta_m,\eta_m) \\
&\bar{v}_x(X > X_m) = -\bar{v}_x(X < X_m) + \frac{4}{3}\left(\frac{\beta}{\beta-1}\right)^{1/2} v_t \frac{p_3(\eta,\eta)}{p_2(\eta_m,\eta_m)} \\
&\quad = \frac{2}{3}\left(\frac{\beta}{\beta-1}\right)^{1/2} \frac{v_t}{p_2(\eta_m,\eta_m)} [p_3(\eta,\eta_m) - (\eta-\eta_m)^{3/2} p_0(0,\eta_m)] \\
&\qquad - v_t [(\eta-\eta_m)/(\beta(\beta-1))]^{1/2} \\
&\overline{v_x^2} = \left(\frac{\beta-1}{\beta}\right) v_t^2 (\eta - \eta_m) + \left(\frac{2\beta+1}{4\beta}\right) v_t^2 \frac{p_4(\eta_m,\eta_m)}{p_2(\eta_m,\eta_m)} \\
&J_y = \pi v_t^4 \beta^{-1/2} p_2(\eta_m,\eta_m) \\
&\overline{v_y}(X > X_m) = -\overline{v_y}(X < X_m) + \frac{4\beta^{1/2}}{3} v_t \frac{p_3(\eta,\eta)}{p_2(\eta_m,\eta_m)} \\
&\quad = \frac{2\beta^{1/2}}{3} \frac{v_t}{p_2(\eta_m,\eta_m)} [p_3(\eta,\eta_m) - (\eta-\eta_m)^{3/2} p_0(0,\eta_m)] \\
&\qquad - v_t(\beta-1)[(\eta-\eta_m)/\beta]^{1/2} \\
&\overline{v_y^2} = \frac{1}{\beta} v_t^2 (\eta - \eta_m) + \frac{(3\beta-1)}{4\beta} v_t^2 \frac{p_4(\eta_m,\eta_m)}{p_2(\eta_m,\eta_m)}
\end{aligned}\right\} \tag{46}$$

These are our final simplified relations, valid for an arbitrary $f_3(w_0^2)$ at the cathode.

When f_3 is a maxwellian distribution, given by eqn. (4), we find that

$$\left.\begin{aligned}
&n/n_T=\exp(\eta)[1\mp\Phi((\eta-\eta_m)^{1/2})] \quad \text{for} \quad X\gtrless X_m\\
&J_x/J_s=\exp(\eta_m)(\beta-1)^{1/2}/\beta^{1/2}\\
&\overline{v_x}/v_t=\frac{\sqrt{\pi}}{2}(\exp(\eta-\eta_m))\left(\frac{\beta}{\beta-1}\right)^{1/2}[1\mp\Phi((\eta-\eta_m)^{1/2})]\\
&\qquad\pm\left[\frac{(\beta-1)}{\beta}(\eta-\eta_m)\right]^{1/2} \quad \text{for} \quad X\gtrless X_m\\
&\overline{v_x^2}/v_t^2=(\beta-1)(\eta-\eta_m)/\beta+1+(2\beta)^{-1}\\
&J_y/J_s=\exp(\eta_m)/\sqrt{\beta}\\
&\overline{v_y}/v_t=\frac{\sqrt{\pi}}{2}(\exp(\eta-\eta_m))\beta^{1/2}[1\mp\Phi((\eta-\eta_m)^{1/2})]\pm(\eta-\eta_m)^{1/2}/\beta^{1/2} \quad \text{for} \quad X\gtrless X_m\\
&\overline{v_y^2}/v_t^2=(\eta-\eta_m)/\beta+\tfrac{3}{2}-(2\beta)^{-1}\\
&\text{where}\\
&\quad v_t^2=2kT/m
\end{aligned}\right\} \tag{47}$$

This set of relations for a maxwellian distribution can also be derived directly upon integration in the cartesian frame (w_{x0}, w_{y0}). The use of the polar frame allows us to derive the relations in eqn. (46) for an arbitrary f_3 distribution function.

The following observations are noteworthy, subject to the assumptions in this section.

(1) The expressions for J_x and J_y are independent of X or $\eta(X)$ and in fact

$$J_y=J_x/(\beta-1)^{1/2}, \quad (J_x^2+J_y^2)^{1/2}=J_s\exp(\eta_m) \tag{48}$$

the latter being identical to the expression in the zero magnetic field case (omitting the η_m dependence on magnetic field). The relation for J_y in eqn. (47) is also given by Lindsay (1970) in his eqn. 5.5. His Fig. 9 also shows that J_y is independent of X over a large range of X values, but because he adopts $\beta=\alpha=2$ with α not large enough to satisfy our conditions, J_y decreases near $X=0$. When $\alpha\gtrsim 3{\cdot}2$, J_y is independent of X even for X approaching zero, provided the conditions, given at the head of this section are also obeyed.

(2) A single relation applies for all X both for $\overline{v_x^2}$ and $\overline{v_y^2}$.

(3) The relation for n is identical to that in a zero magnetic field case. This expression can be thought of as the '*second approximation*' to the density profile, since inserting a parabolic potential ($d^2\eta/dX^2=2\beta$) into Poisson's equation, $d^2\eta/dX^2=(2e/m\omega_c^2)d^2\phi_0/dx^2=2e^2n/m\omega_c^2\varepsilon_0$, implies that n is a constant in the 'first approximation' given by

$$n=\beta m\omega_c^2\varepsilon_0/e^2 \quad \text{or} \quad \omega_p^2/\omega_c^2=\beta \tag{49}$$

where $\omega_p=(ne^2/\varepsilon_0 m)^{1/2}$ is the plasma frequency†. Using the second approximation

† We note that when $n=n_T$ (see eqn. (4)), β is equal to $\kappa^{-2}=\xi^2/X^2$, where κ and ξ are defined in Lindsay and Goodwell (1965).

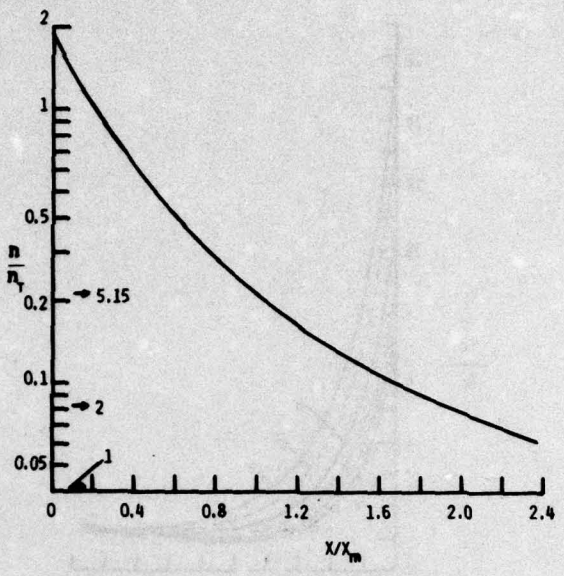

Figure 4. Normalized electron density versus X/X_m when $\phi_m = -0{\cdot}155$ V and $T = 1160$ K, or $\eta_m = -1{\cdot}55$. The arrows indicate 'effective' values of β when for example $eJ_s = 1{\cdot}69 \times 10^4$ A/m^2, $B_0 = 650$ G and $x_m = 9 \times 10^{-6}$ m.

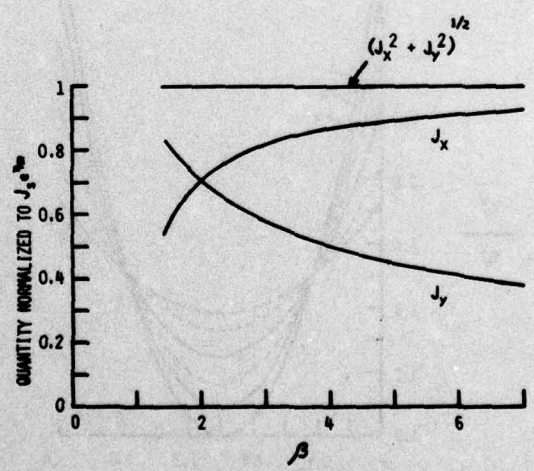

Figure 5. The current density fluxes $J_x/[J_s \exp(\eta_m)]$ and $J_y/[J_s \exp(\eta_m)]$ and their r.m.s. sum versus β.

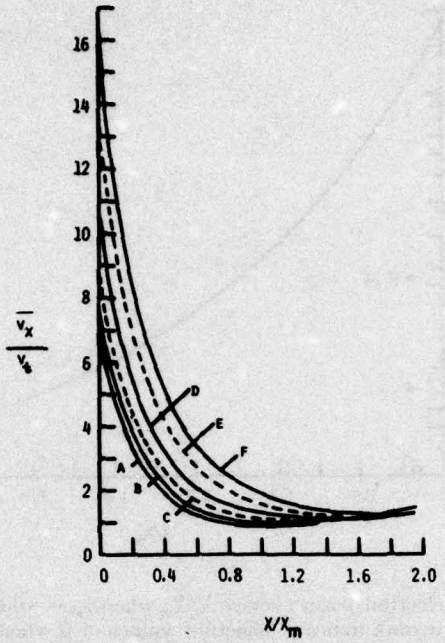

Figure 6. Profile of $\bar{v}_x/v_t$ versus X/X_m when $\eta_m = -1{\cdot}55$. Curves correspond to β values (A) 200, (B) 6, (C) 3·085, (D) 2, (E) 1·480 and (F) 1·3.

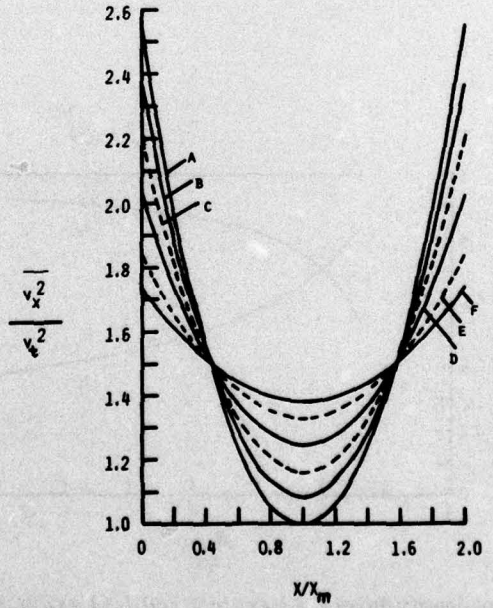

Figure 7. Profile of $\overline{v_x^2}/v_t^2$ versus X/X_m when $\eta_m = -1{\cdot}55$. Curves correspond to β values (A) 200, (B) 6, (C) 3·085, (D) 2, (E) 1·480 and (F) 1·3.

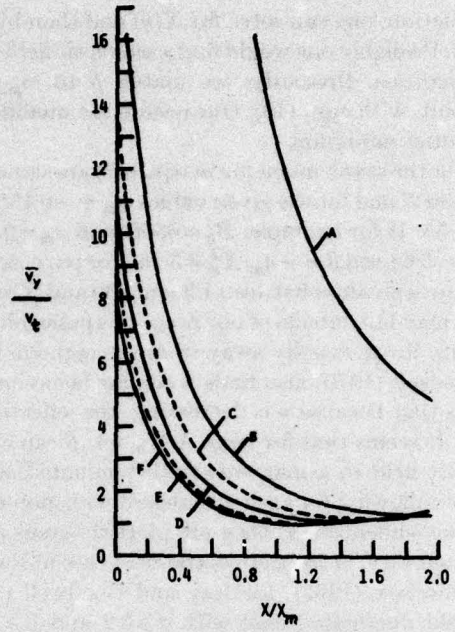

Figure 8. Profile of $\bar{v}_y/v_i$ versus X/X_m when $\eta_m = -1{\cdot}55$. Curves correspond to β values (A) 200, (B) 6, (C) 3·085, (D) 2, (E) 1·480 and (F) 1·3.

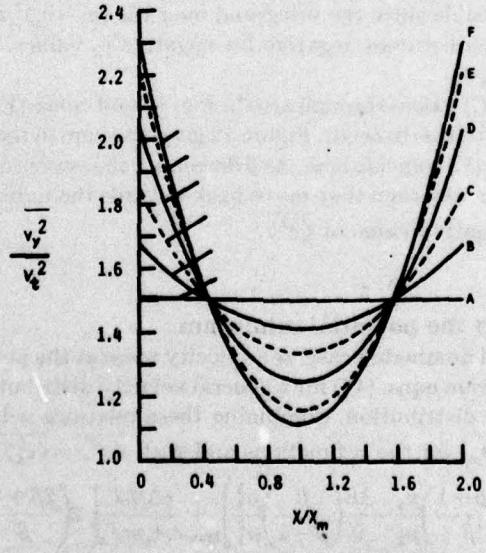

Figure 9. Profile of $\overline{v_y^2}/v_i^2$ versus X/X_m when $\eta_m = -1{\cdot}55$. Curves correspond to β values (A) 200, (B) 6, (C) 3·085, (D) 2, (E) 1·480 and (F) 1·3.

for n and Poisson's equation, one can solve for $X(\eta)$ and thereby effect an iteration process (not done here). Probably one would find a magnetic field dependence for n in higher-order approximations. Presently, we match β to ω_{pm}, its value at the potential minimum point, with eqn. (49). Our results are qualified to apply only in the region of the potential minimum.

Calculated results for the seven moments in eqn. (47) are shown in Figs. 4–9 up to X/X_m values just beyond 2, and for the given values $\phi_m = -0{\cdot}155$ V and $T = 1160$ K, equivalent to $\eta_m = -1{\cdot}55$. If for example, $B_0 = 650$G and $x_m = 9 \times 10^{-6}$ m, then $X_m = 0{\cdot}549$, $\alpha = -2\eta_m/X_m = 5{\cdot}65$ and $\beta = -\eta_m/X_m^2 = 5{\cdot}15$. For purposes of illustration, we allow in some of the figures β values between 1·3 and 200 and X values down to zero, although some regions may fall outside of our range of applicability. Figure 4 shows that the electron density drops rapidly away from the cathode but decreases more slowly beyond X_m. Lindsay (1970) also finds a similar behaviour.

Figure 4 also shows that because n is decreasing, the 'effective β' given by eqn. (49) is also decreasing. It seems that for large $X/X_m \gg 1$, β can change from $\beta > 1$ to $\beta < 1$ or from an electric-field to a magnetic-field dominated situation within the same diode. An analysis allowing for such a change-over is non-existent at present. Since J_x and J_y are independent of X, they are plotted versus β in Fig. 5. For the magnetic-field dominated case, or for the electric-field case at low α and β, J_y varies with X as shown in Lindsay (1962), Lindsay and Goodwell (1965) and Lindsay (1970). The electric-field dominated case with $\alpha \geqslant 3{\cdot}2$ and $\beta \geqslant 1{\cdot}5$ seems to differ greatly. Figures 7 and 9 show that $\overline{v_x^2}$ and $\overline{v_y^2}$ are symmetric about the X_m point and vary by a much lesser degree than $\overline{v_x}$ and $\overline{v_y}$. Figure 8 indicates that $\overline{v_y}$ becomes very large as β increases, in contrast to $\overline{v_x}$ in Fig. 6 which decreases with β.

In Figs. 10 and 11, we plot the profiles of $\overline{\langle v_x^2 \rangle}$ and $\overline{\langle v_y^2 \rangle}$ defined in eqn. (7). The two behave differently for small X and large β. The former becomes less negative whereas the latter becomes exceedingly negative. Negative values indicate that $\bar{v}_x > (\overline{v_x^2})^{1/2}$, which is possible since the integrand over the $(v_x - \bar{v}_x)^2$ average contains the product $v_x f_3$, which becomes negative for negative v_x values. Similar remarks apply to the v_y averages.

At $X = X_m$, curve (C) passes through zero in Fig. 10 and curve (E) in Fig. 11, their β values being chosen for this to occur. Figure 12 gives the sum of the plots in Figs. 10 and 11. Curves (C) and (E) coincide here. As β decreases, the curves move towards the left until β is equal to 2, and then they move back towards the right. The $\beta = 2$ curve (D) gives the least negative value of $\overline{\langle v^2 \rangle}$.

7. Velocity noise at the potential minimum

In the electric-field dominated case, the velocity noise at the potential minimum is readily obtainable from eqns. (46) for a general velocity distribution function and (47) for a maxwellian distribution. Combining these relations with eqn. (7) yields with arguments (η_m, η_m) for the p functions and with $\overline{\langle v^2 \rangle} = \overline{\langle v_x^2 \rangle} + \overline{\langle v_y^2 \rangle}$:

$$\overline{\langle v_x^2 \rangle} = \frac{e\Delta f \bar{v}_i^2}{2eA_e J_x}\left[\left(\frac{2\beta+1}{\beta}\right)\frac{p_4}{p_2} - \frac{16}{9}\left(\frac{\beta}{\beta-1}\right)\frac{p_3^2}{p_2^2}\right] \underset{\text{Max.}}{\rightarrow} \frac{e\Delta f kT}{eA_e m J_x}\left[2\left(\frac{2\beta+1}{\beta}\right) - \frac{\pi\beta}{\beta-1}\right] \quad (50)$$

$$\overline{\langle v_y^2 \rangle} = \frac{e\Delta f \bar{v}_i^2}{2eA_e J_y}\left[\left(\frac{3\beta-1}{\beta}\right)\frac{p_4}{p_2} - \frac{16}{9}\beta\frac{p_3^2}{p_2^2}\right] \underset{\text{Max.}}{\rightarrow} \frac{e\Delta f kT}{eA_e m J_y}\left[2\left(\frac{3\beta-1}{\beta}\right) - \pi\beta\right] \quad (51)$$

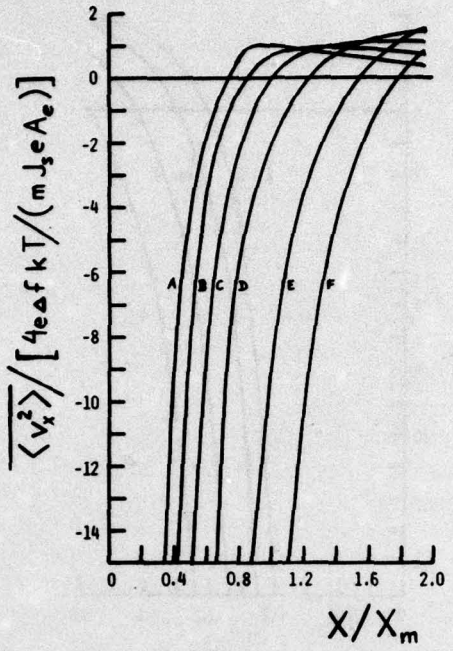

Figure 10. Normalized velocity noise component, $\overline{\langle v_x^2 \rangle}$, versus X/X_m when $\eta_m = -1{\cdot}55$. Curves correspond to β values (A) 200, (B) 6, (C) 3·085, (D) 2, (E) 1·480 and (F) 1·3.

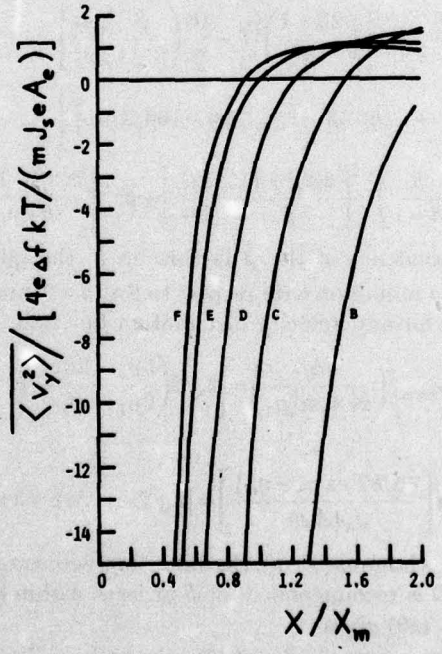

Figure 11. Normalized velocity noise component, $\overline{\langle v_y^2 \rangle}$ versus X/X_m when $\eta_m = -1{\cdot}55$. Curves correspond to β values (B) 6, (C) 3·085, (D) 2, (E) 1·480 and (F) 1·3.

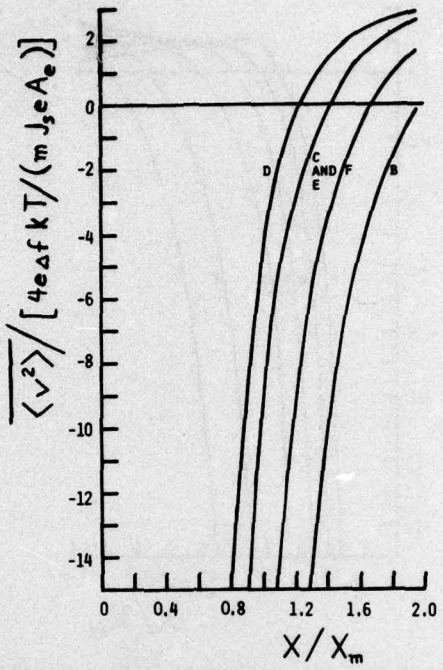

Figure 12. Normalized velocity noise sum, $\overline{\langle v^2\rangle}=\overline{\langle v_x^2\rangle}+\overline{\langle v_y^2\rangle}$, versus X/X_m when $\eta_m=-1{\cdot}55$. Curves correspond to β values (B) 6, (C) 3·085, (D) 2, (E) 1·480 and (F) 1·3.

$$\overline{\langle v^2\rangle}=\frac{e\Delta f}{2eA_e\pi v_i^2 p_2}\left\{\left(\frac{\beta}{\beta-1}\right)^{1/2}\left[\left(\frac{2\beta+1}{\beta}\right)\frac{p_4}{p_2}-\frac{16}{9}\left(\frac{\beta}{\beta-1}\right)\frac{p_3^2}{p_2^2}\right]\right.$$

$$\left.+\sqrt{\beta[(3\beta-1)p_4/\beta p_2-16\beta p_3^2/9p_2^2]}\right\}$$

$$\underset{\text{Max.}}{\rightarrow}\frac{e\Delta fkT}{J_s eA_e m}\exp(-\eta_m)\left\{\left(\frac{\beta}{\beta-1}\right)^{1/2}\left[\frac{2(2\beta+1)}{\beta}-\frac{\pi\beta}{\beta-}\right]+\beta^{1/2}\left[\frac{2(3\beta-1)}{\beta-1}-\pi\beta\right]\right\} \tag{52}$$

Omitting the slight dependence of the p factors on β, the quantity within the parenthesis in $|\overline{\langle v^2\rangle}|$ has a minimum with respect to β at $\beta=2$, and this occurs when $\langle v_x^2\rangle=\langle v_y^2\rangle$. This is true for any velocity distribution function. Then

$$|\overline{\langle v^2\rangle}|_{\min}\Big/\left(\frac{e\Delta f}{2eA_e\pi v_i^2 p_2}\right)=\left|2\sqrt{2}\left(\frac{5p_4}{2p_2}-\frac{32p_3^2}{9p_2^2}\right)\right| \tag{53}$$

For a maxwellian

$$|\overline{\langle v^2\rangle}|_{\min}\Big/\left[\frac{e\Delta fkT\exp(-\eta_m)}{J_s eA_e m}\right]=|2\sqrt{2}(5-2\pi)|=3{\cdot}629 \tag{54}$$

At best this is 4·23 times as large as $(4-\pi)$, the value for a zero magnetic-field case. In practice, a value of $\beta=2$ is recommended, or β at least within the limits 1·5 to 3. Inserting $\beta=2$ into eqn. (49) gives

$$\omega_{pm}^2/\omega_c^2=2 \tag{55}$$

This is the desired relation for minimum velocity noise at the potential minimum.

In terms of the alternate relationships, $\beta = -\eta_m/X_m^2$ and $\alpha = -2\eta_m/X_m$, the conditions $\beta = 2$ and $\alpha \geqslant 3{\cdot}2$ imply that we want $X_m \geqslant 0{\cdot}8$ and $|\eta_m| = 2X_m^2 > 1{\cdot}28$.

Van Duzer (1963) uses the magnetic field independent factors $(4-\pi)$ and 2 respectively for $\overline{\langle v_x^2 \rangle}$ and $\overline{\langle v_y^2 \rangle}$. In contrast, our analysis provides the magnetic field dependent factors in eqns. (50)–(52).

Figure 13 shows the normalized variations of $\overline{\langle v_x^2 \rangle}$, $\overline{\langle v_y^2 \rangle}$ and $\overline{\langle v^2 \rangle}$ versus β at the potential minimum. The $\overline{\langle v_x^2 \rangle}$ quantity, normalized as shown, increases from large negative values and tends towards $(4-\pi)$ as β becomes large. The $\overline{\langle v_y^2 \rangle}$ normalized quantity decreases to large negative values as β becomes large. The sum $\overline{\langle v^2 \rangle}$ is least in magnitude at $\beta = 2$, decreasing to large negative values for larger and smaller β. Since $\overline{\langle v^2 \rangle}$ is associated directly with velocity noise at the potential minimum, the main conclusion of this analysis is to operate the diode by adjusting B and T so that $\omega_{pm}/\omega_c^2 = 2$ is satisfied.

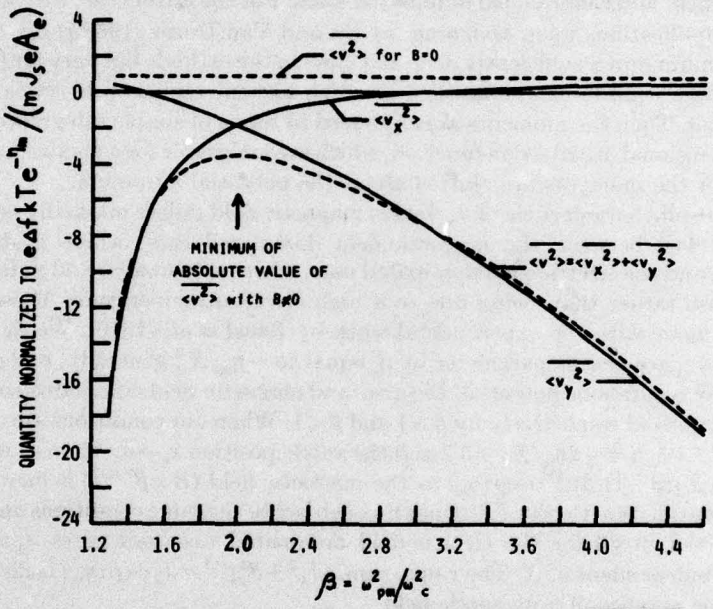

Figure 13. Variations of normalized velocity noise components, $\overline{\langle v_x^2 \rangle}$, $\overline{\langle v_y^2 \rangle}$ and their sum $\overline{\langle v^2 \rangle}$ versus β at the potential minimum.

8. Conclusions

We analyse both the magnetic-field and electric-field dominated cases in a thermionic diode with crossed electric and magnetic fields. Assuming a parabolic spatial variation in potential about the space-charge minimum, we clarify several aspects and obtain simple but important results for the noise in the velocity components.

In §§3 and 4, we illuminate Lindsay's (1960, 1964) considerations on the velocity regions over which one has to integrate the velocity distribution functions to derive the moments integrated over the distribution. We show the following:

(*a*) The ω_{x0C} curve is tangent to both the w_{x0A} and w_{x0B} curves in a (w_{x0}, w_{y0}) plot (see eqns. (10) and (24)) under electric-field dominated conditions.

(*b*) The regions and limits of integration are mapped and their equivalences in the (w_x, w_y) and (w_{x0}, w_{y0}) planes are identified, both in the electric-field and magnetic-field dominated situations.

For the electric-field dominated case, Lindsay (1964) could not proceed before the potential distribution was known. Upon assuming a parabolic variation about the potential minimum, we illustrate in § 5, the following, also noted by Lindsay (1970):

(*a*) Our formula reduces to Lindsay's (1964), if a parabolic potential variation is inserted into Lindsay's equation.

(*b*) The result of Ho and Van Duzer (1968 a), also for a parabolic variation, agrees with our result if we allow the anode to recede to infinity, as they do. Our formula is more general in that it allows the velocity distribution function at the cathode to be an arbitrary function of $w_{x0}^2 + w_{y0}^2 + w_{z0}^2$.

General relations are derived for seven moments in terms of integrals over the arbitrary two-dimensional electron velocity distribution function, both for the magnetic-field and electric-field dominated cases. For the latter case, we effect in § 6 major simplifications upon assuming, as Ho and Van Duzer (1968 a) do, that the potential minimum is sufficiently deep and close to the cathode but very far from the anode. These conditions are satisfied for high current emission densities in high power tubes. Then the moments are expressed in terms of simple integrals over the three-dimensional distribution function, which are integrable for a maxwellian form. Profiles for the moments are plotted about the potential minimum.

The cut-off characteristic of J_x versus magnetic field differs markedly (see eqns. (22) and (44)) between the magnetic-field dominated case, where it decreases abruptly, and the electric-field dominated case, where it is broader and indicative of such a case rather than being due to a high electron temperature. These cut-off concepts agree with the experimental work by Bacal *et al.* (1970). We denote the important space-charge parameter by β, equal to $-\eta_m/X_m^2$ generally, and given by ω_{pm}^2/ω_c^2 for a parabolic potential. Electric- and magnetic-field dominated conditions are characterized respectively by $\beta > 1$ and $\beta < 1$. When our conditions are satisfied, namely $\beta \geqslant 1{\cdot}5$, $\alpha = -2\eta_m/X_m \geqslant 3{\cdot}2$ and the anode position $x_a \to \infty$, than J_x decreases slowly as $J_s[(\beta-1)/\beta)]^{1/2} \exp(\eta_m)$ as the magnetic field ($B \propto \beta^{-1/2}$) is increased.

The new relation for the J_y current flux subject to the same conditions on α, β and x_a is derived in § 6 for the electric-field dominated case and gives $J_y = J^s \beta^{-1/2} \exp(\eta_m)$, independent of X. The r.m.s. sum, $(J_x^2 + J_y^2)^{1/2} = J_x \exp(\eta_m)$ is identical to that in the absence of a magnetic field.

From the relations for the velocity moments, $\bar{v}_{x,y}$ and $\overline{v_{x,y}^2}$, we obtain, using Rack's (1938) method, the noise velocity components $\overline{\langle v_{x,y}^2 \rangle}$ in terms of the mean square deviations, $\overline{v_{x,y}^2} - (\bar{v}_{x,y})^2$, and in particular their values at the potential minimum. The results are illustrated in Fig. 13. In the absence of a magnetic field, $\overline{\langle v^2 \rangle}$ has the multiplicative factor $(4-\pi)$. In crossed electric and magnetic fields, both $\overline{\langle v_{x,y}^2 \rangle}$ components depend on magnetic field through the β factor. The sum $|\overline{\langle v_x^2 \rangle} + \overline{\langle v_y^2 \rangle}|$ has a minimum at $\beta = 2$ and its multiplicative factor is $|2\sqrt{2(5-2\pi)}|$ which is 4·23 times worse than the zero-magnetic field case. For optimum operation, one should adjust $\beta = \omega_{pm}^2/\omega_c^2 = 2$. In all cases, the velocity noise is also proportional to the cathode temperature. If the tube can be operated with no cathode heater, this broad-band noise will be greatly reduced. This probably explains the experiments of Bespalov and Usychenko (1976) and Bespalov *et al.* (1976).

Acknowledgment

This research was sponsored by the Air Force Office of Scientific Research (AFSC), United States Air Force, under Contract No. F49620-77-C-0106. The United States Government is authorized to reproduce and distribute reprints for government purposes notwithstanding any copyright notation therein.

Appendix

Simplification of expressions for case in §6.

We keep the first term of $G_{\alpha,A}$ in eqn. (36), the first two terms of $G_{\alpha,B}$ in (37) and the first three terms of $G_{\alpha,C}$ in (38). We wish to transform these three approximated relations to yield the results in eqn. (46).

Define

$$X_0 = X - X_m \quad \text{and} \quad s^2 = w^2 - w_{0b}^2 = w^2 - \alpha^2/4\beta = w^2 + \eta_m$$

The following equality is particularly useful:

$$[w^2+\eta-(wZ_{4,5}+X)^2]^{1/2} = \beta^{-1/2}s \mp (\beta-1)^{1/2}|X_0|\,\mathrm{Sign}\,(X_0) \quad \text{if} \quad w^2 \geqslant w_{0d}^2$$
$$= |X_0|(\beta-1)^{1/2} \mp \beta^{-1/2}s\,\mathrm{Sign}\,(X_0) \quad \text{if} \quad w^2 \leqslant w_{0d}^2$$

where Sign stands for the sign, so that $\mathrm{Sign}\,(X - X_m) = \pm 1$ depending on whether $X \gtrless X_m$. Each moment has to be considered separately and integrated by parts.

It is convenient in the intermediate algebra to define $F(w^2)$ and $F_D(x^2)$ functions, given by $\partial F(w^2)/\partial w \equiv -2wf_2(w^2)$ and $\partial F_D(w^2)/\partial w \equiv -2wF(w^2)$, to be used in the integration by parts. After considerable algebra, one obtains the following results for the approximated forms of eqns. (36) to (38).

$$G_{0,B} = \sqrt{\beta}|X_0| \int_0^\infty ds\, F(s^2+w_{0b}^2)/(s^2+\beta X_0^2), \quad \text{if } X_0 > 0$$

$$G_{0,C} = \pi F(w_{0a}^2) - G_{0,B}, \quad \text{if } X_0 < 0$$

$$G_{1,A} = 2\left(\frac{\beta-1}{\beta}\right)^{1/2} \int_0^\infty ds\, s^2 f_2(s^2+{w_{0b}}^2)$$

$$G_{2,B} = \tfrac{1}{2}\beta^{1/2}|X_0|\left[\int_0^\infty ds\, F(s^2+w_{0b}^2) + \int_0^\infty \frac{ds\, F_D(s+w_{0b}^2)}{s^2+\beta X_0^2}\right]$$
$$+ |X_0|(\beta-2)\beta^{-1/2} \int_0^\infty ds\, s^2 f_2(s^2+w_{0b}^2), \quad \text{if } X_0 > 0$$

$$G_{2,C} = \frac{\pi}{2} F_D(w_{0a}^2) - G_{2,B}, \quad \text{if } X_0 < 0$$

$$G_{3,A} = \frac{2}{3}\left(\frac{\beta-1}{\beta}\right)^{1/2} \int_0^\infty ds\, s^2 f_2(s^2+w_{0b}^2)\left[s^2\left(\frac{2\beta+1}{\beta}\right) + 3X_0^2(\beta-1)\right]$$

$$G_{4,B} = G_{4,C} = 2\beta^{-1/2} \int_0^\infty ds\, s^2 f_2(s^2+w_{0b}^2)$$

$$G_{5,B} = (1/2)\,\beta^{1/2}|X_0|\left[\int_0^\infty ds\, F(s^2+w_{0b}^2) + \int_0^\infty \frac{ds\, F_D(s^2+w_{0b}^2)}{s^2+\beta X_0^2}\right]$$

$$-|X_0|(\beta-2)\beta^{-1/2}\int_0^\infty ds\, s^2 f_2(s^2+w_{0b}^2), \quad \text{if } X_0>0$$

$$G_{5,C}=\frac{\pi}{2}F_D(w_{0a}^2)-G_{5,B}, \quad \text{if } X_0<0$$

$$G_{6,B}=G_{6,C}=2\beta^{-1/2}\int_0^\infty ds\, s^2 f_2(s^2+w_{0b}^2)[X_0^2+s^2(3\beta-1)/3\beta]$$

All the above integrals over f_2, F and F_D can be transformed to integrals over f_3, the standard three-dimensional distribution function in eqn. (3). The following identities which can be easily proven can be substituted into the above relations to yield the results in eqn. (46).

$$\int_0^\infty ds\, s^2 f_2(s^2+w_{0b}^2)=\frac{\sqrt{\pi}}{2}\int_0^\infty dw\, w^3 f_3(w^2+w_{0b}^2)$$

$$\int_0^\infty ds\, s^4 f_2(s^2+w_{0b}^2)=\frac{3\sqrt{\pi}}{8}\int_0^\infty dw\, w^5 f_3(w^2+w_{0b}^2)$$

$$\int_0^\infty ds\, F(s^2+w_{0b}^2)=\sqrt{\pi}\int_0^\infty dw\, w^3 f_3(w^2+w_{0b}^2)$$

$$\int_0^\infty \frac{ds\, F(s^2+w_{0b}^2)}{s^2+\beta X_0^2}=2\sqrt{\pi}\int_0^\infty dw\, w f_3(w^2+w_{0b}^2)\left[\left(\frac{w^2+\beta X_0^2}{\beta X_0^2}\right)^{1/2}-1\right]$$

$$F_D(w_{0a}^2)=\frac{8}{3\sqrt{\pi}}\int_0^\infty dw\, w^4 f_3(w^2+w_{0a}^2)$$

$$\int_0^\infty \frac{ds\, F_D(s^2+w_{0b}^2)}{s^2+\beta X_0^2}=\frac{4\sqrt{\pi}}{3}\int_0^\infty dw\, w f_3(w^2+w_{0b}^2)\left[\frac{(w+\beta X_0^2)^{3/2}}{(\beta X_0^2)^{1/2}}-\beta X_0^2-\frac{3}{2}w^2\right]$$

References

Bacal, M., Critescu, M., and Voci, C., 1970, *Int. J. Electron.*, **28**, 149.

Bespalov, A. N., Kandybei, V. G., Nekrasov, L. G., and Usychenko, V. G., 1976, *Soviet Phys. tech. Phys.*, **21**, 882.

Bespalov, A. N., and Usychenko, V. G., 1976, *Soviet Phys. tech. Phys.*, **21**, 881.

Ho, R. Y. C., and Van Duzer, T., 1968 a, I.E.E.E. *Trans Electron Devices*, **15**, 70; 1968 b, *Ibid.*, **15**, 75.

Lindsay, P. A., 1960, *J. Electron. Control*, **8**, 177; 1964, *Ibid.*, **17**, 67; 1962, *J. appl. Phys.*, **33**, 3298; 1970, *Proc. R. Soc.*, A, **315**, 479.

Lindsay, P. A., and Goodwell, R. S., 1965, *J. appl. Phys.*, **36**, 411.

Rack, A. J., 1938, *Bell Syst. tech. J.*, **17**, 592.

Smullin, L. D., and Haus, H. A., 1959, *Noise in Electronic Devices* (N.Y.: MIT Press and Wiley & Sons), p. 18.

Van Duzer, T., 1963, I.E.E.E. *Trans. Electron. Devices*, **10**, 370.